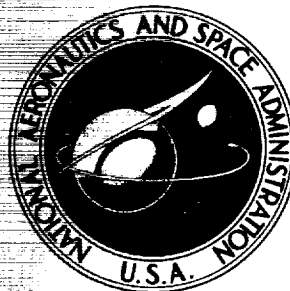


~~CONFIDENTIAL~~

UB

NASA TM X-2253

NASA TECHNICAL
MEMORANDUM



~~NOFORN~~

DOWNGRADED TO UNCL-----
BY AUTHORITY OF NASA CLASSIFICATION
CHANGE NOTICES NO 241 DATED 31-06-76
ITEM NO. 15-----

CASE
CONFIDENTIAL

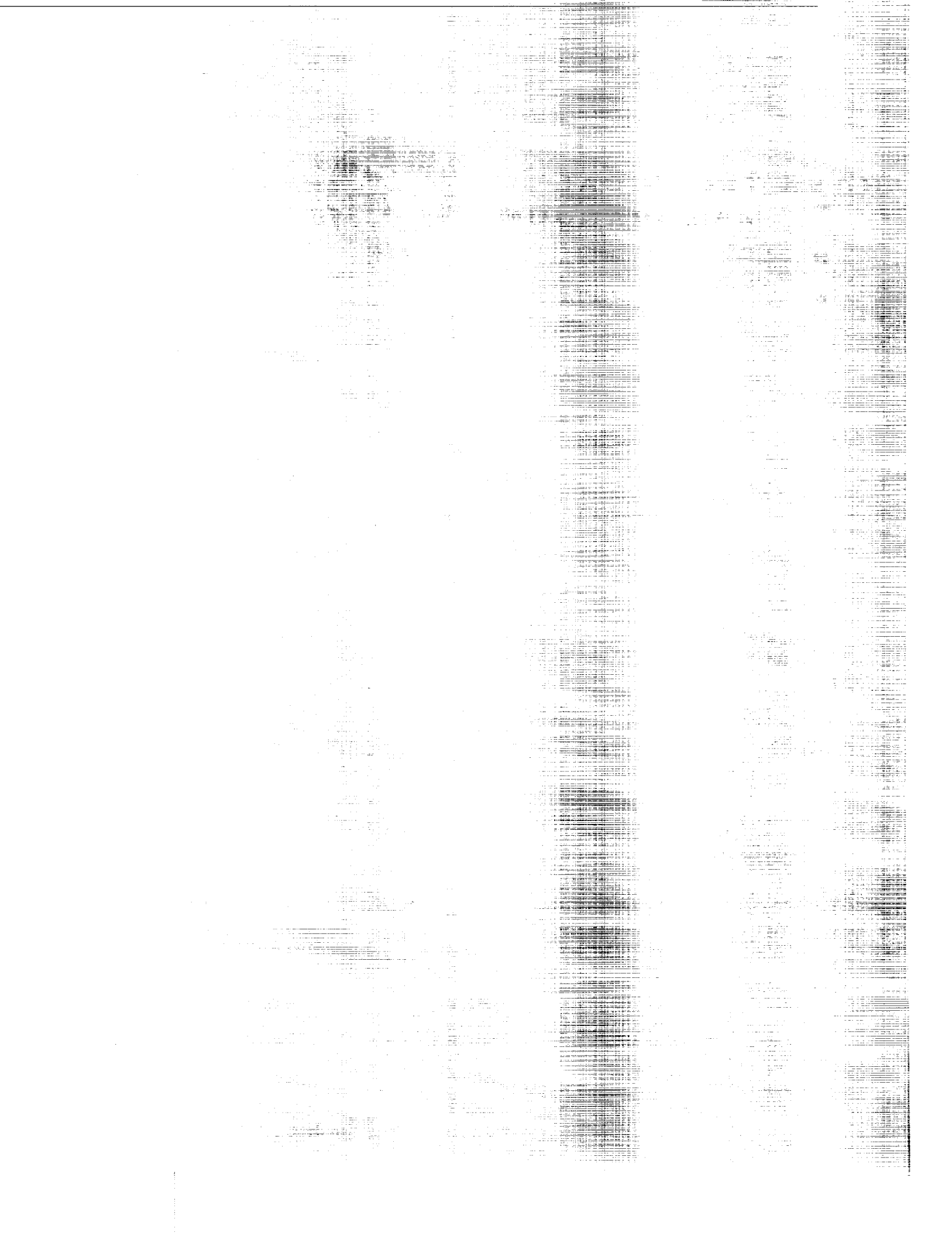
FLIGHT MEASUREMENTS OF
BOUNDARY-LAYER TRANSITION
ON A 5° HALF-ANGLE CONE AT
FREE-STREAM MACH NUMBER
OF 20 (REENTRY F)

by Robert L. Wright and Ernest V. Zoby
Langley Research Center
Hampton, Va. 23365

TO UNCLASSIFIED
By authority of NASA
Classified by 0-100000-10 Date 9/4/76
Classified Document Master Control Station, NASA
Scientific and Technical Information Facility

NATIONAL AERONAUTICS AND SPACE ADMINISTRATION • WASHINGTON, D. C. • MAY 1971

~~CONFIDENTIAL~~



~~CONFIDENTIAL~~

1. Report No. NASA TM X-2253	2. Government Accession No. C71 843	3. Recipient's Catalog No.
4. Title and Subtitle FLIGHT MEASUREMENTS OF BOUNDARY-LAYER TRANSITION ON A 5° HALF-ANGLE CONE AT A FREE- STREAM MACH NUMBER OF 20 (REENTRY F) (U)	5. Report Date May 1971	6. Performing Organization Code
7. Author(s) Robert L. Wright and Ernest V. Zoby	8. Performing Organization Report No. L-7506	10. Work Unit No. 711-02-09-01
9. Performing Organization Name and Address NASA Langley Research Center Hampton, Va. 23365	11. Contract or Grant No.	13. Type of Report and Period Covered Technical Memorandum
12. Sponsoring Agency Name and Address National Aeronautics and Space Administration Washington, D.C. 20546	14. Sponsoring Agency Code	
15. Supplementary Notes		
16. Abstract <p>Experimental free-flight transition data have been obtained on a slightly blunted 5° half-angle cone at a free-stream Mach number of 20. The locations of the beginning and end of transition were determined by the intersection of curves faired through the laminar, transitional, and turbulent heating-rate data. The temperature-history technique for determining transition as currently used (sharp break in curve) and the heating-rate-history technique were compared with the heating-rate-distribution transition results. The experimental data, when presented in the form of local Reynolds numbers and Mach number, were shown to have trends similar to those existing in wind-tunnel data.</p> <p>CLASSIFIED BY ET/MD (10/1/72) NASA-2431 SUBJECT TO GENERAL DECLASSIFICATION SCHEDULE OF EXECUTIVE ORDER 11652. AUTOMATICALLY DECLASSIFIED AT TWO-YEAR INTERVALS. DECLASSIFIED ON DECEMBER 31, 1977</p>		
17. Key Words (Suggested by Author(s)) Free flight Slightly blunted cone Boundary-layer transition Laminar, transitional, and turbulent heating data	18. Distribution Statement Confidential Available to U.S. Government Agencies and Their Contractors Only	
19. Security Classif. (of this report) Confidential Group 4	20. Security Classif. (of this page) Unclassified	21. No. of Pages 38
22. Price		
23. Other Notes GROUP 4 Downgraded at 2 year intervals; declassified after 12 years		24. This material contains information affecting the national defense of the United States within the meaning of the espionage laws, Title 18, U.S.C. Sec. 793 and 794, the transmission or revelation of which in any manner to an unauthorized person is prohibited by law.

~~CONFIDENTIAL~~

~~CONFIDENTIAL~~

FLIGHT MEASUREMENTS OF BOUNDARY-LAYER TRANSITION
ON A 5° HALF-ANGLE CONE AT A FREE-STREAM
MACH NUMBER OF 20 (REENTRY F)*

By Robert L. Wright and Ernest V. Zoby
Langley Research Center

SUMMARY

Experimental free-flight transition data have been obtained on a 3.962-m- (13-foot-) long, 5° half-angle cone with an initial nose radius of 0.254 cm (0.10 inch). The data were obtained during reentry from altitudes of approximately 30.480 to 18.288 km (100 000 to 60 000 feet) at a free-stream Mach number of 20. The free-stream Reynolds number varied from 6.56×10^6 to 52.5×10^6 per meter (2.0×10^6 to 16.0×10^6 per foot), and the total enthalpy from about 18.3 to 16.9 MJ/kg (7900 to 7300 Btu/lbm). The locations of the beginning and end of transition were determined by the intersection of curves faired through the laminar, transitional, and turbulent heating-rate data. The temperature-history technique for determining transition as currently used (sharp break in curve) was shown to compare unfavorably with the heating-rate-distribution method. The heating-rate-history technique, which is proportional to the temperature derivative and consequently more sensitive to perturbations, gives better agreement with the heating-rate-distribution transition results. Transition was observed to occur farther forward on the windward ray than on the leeward ray. The experimental data, when presented in the form of local Reynolds numbers and Mach number, were shown to have trends similar to those existing in wind-tunnel data.

INTRODUCTION

A 3.962-m (13-ft) conical body, with a half-angle of 5° and an initial nose radius of 0.254 cm (0.10 in.), was flown to extend turbulent heat-transfer data to conditions of high local Reynolds number and Mach number. The flight test, designated "Reentry F," also provided experimental data on boundary-layer transition during reentry. A preliminary analysis of the heating and transition measurements was published in reference 1. Detailed analyses of the experimental temperatures and heating rates, surface pressures, angle of attack, and thermal distortion were published in references 2 to 5, respectively.

*~~CONFIDENTIAL~~ Unclassified.


~~CONFIDENTIAL~~

This paper presents the experimental results obtained for the beginning and end of boundary-layer transition during reentry from an altitude of approximately 30.480 to 18.288 km (100 000 to 60 000 ft) at a free-stream Mach number of 20 and a ratio of wall temperature to total temperature of about 0.1. The free-stream Reynolds number varied from about 6.56×10^6 to 52.5×10^6 per meter (2.0×10^6 to 16.0×10^6 per ft), and the corresponding total enthalpy varied from about 18.3 to 16.9 MJ/kg (7900 to 7300 Btu/lbm). The effects of detection techniques, bluntness, and angle of attack are discussed.

SYMBOLS

Values are given in both SI and U.S. Customary Units. The measurements and calculations were made in U.S. Customary Units.

h	altitude
H	total enthalpy
M	Mach number
\dot{q}	heating rate
r	nose radius
Re_x	local Reynolds number
V	velocity
x	axial length
α	angle of attack in thermal-sensor plane ($\phi = 0^\circ, 180^\circ$)
β	angle of attack in plane perpendicular to thermal-sensor plane ($\phi = 90^\circ, 270^\circ$)
δ^*	boundary-layer displacement thickness
η	total angle of attack
θ	boundary-layer momentum thickness


 ϕ circumferential angle

Subscripts:

e local conditions

tr transition

w wall condition

∞ free stream

EXPERIMENT

Spacecraft Description

Pertinent dimensions of the spacecraft are shown in figure 1. Details of the spacecraft structure, design considerations, and internal equipment are given in reference 1. The spacecraft was a 5° half-angle cone, 396.2 cm (156 in.) long with an initial nose-tip radius of 0.254 cm (0.10 in.). The spacecraft structure, 1.524-cm- (0.6-in.-) thick beryllium, served as a calorimeter for the thermal measurements. The graphite nose tip, with an initial tip radius of 0.254 cm (0.10 in.), was installed forward of station 21.84 cm (8.60 in.).

Instrumentation

The prime experimental data obtained on the spacecraft during reentry consisted of temperature measurements of the beryllium wall at the 21 locations (fig. 1) on the spacecraft. There were 12 measurement stations along the primary ray ($\phi = 0^\circ$) and five stations along the diametrically opposite secondary ray ($\phi = 180^\circ$). In addition, thermal sensors are located at the 90° and 270° circumferential positions at stations 185.4 and 365.7 cm (73.0 and 144.0 in.). The sensor at station 73.0, $\phi = 270^\circ$, was inoperative at launch and did not function during the flight.

At each temperature measurement station four chromel-alumel thermocouples were spaced in depth through the beryllium calorimeter skin. The outermost thermocouple was located approximately 0.0254 cm (0.010 in.) beneath the surface of the skin. Details of the construction and assembly of the thermocouple installation are given in reference 1.

Thirteen pressure orifices were also located on the spacecraft to aid in defining the local flow conditions along the spacecraft, and the locations of the pressure sensors

are shown in figure 1. The four heat gages and two pressure orifices shown in figure 1 on the base of the spacecraft were installed to aid in defining the thermal environment in the base region.

Trajectory

Meteorological measurements of atmospheric temperature and pressure in the reentry area were obtained by balloonsonde and rocketsonde payloads. Ambient values of density, coefficient of viscosity, and speed of sound as a function of altitude were derived from these measurements. Altitude and velocity histories of the spacecraft reentry trajectory are shown in figures 2(a) and 2(b). The variations of free-stream Mach number and unit Reynolds number with time during the reentry phase are presented in figures 2(c) and 2(d), respectively.

Angle of Attack

Angle-of-attack components α and β and total angle of attack η are shown in figure 3. The procedure for determining the components from onboard measurements of pitch, yaw, roll rate, and normal and transverse accelerations by using Newtonian aerodynamic coefficients, trajectory, and meteorological data is detailed in reference 4.

The spacecraft experienced thermal distortion along the longitudinal axis as a result of temperature differences on opposite sides of the body due to angle of attack during reentry. At altitudes of less than about 25.908 km (85 000 ft), temperatures along the primary ray $\phi = 0^\circ$ (which was the leeward side) were lower than those at the diametrically opposite secondary ray $\phi = 180^\circ$ (windward side). The calculations of reference 5 which include thermal distortion effects indicate that the local angles of attack along the body differ from those presented in figure 3 by as much as approximately 0.6° at station 40.6 cm (16.0 in.) and 0.1° at the base at an altitude of 18.288 km (60 000 ft).

Local Conditions

Because of the recession of the nose tip during reentry, the local flow properties for the laminar boundary layer were obtained from the blunt-nose equilibrium-air inviscid flow field and the iterative boundary-layer solution (with variable entropy effects) of reference 6. The calculations for turbulent boundary layer are based on a solution of the integral momentum equation with the initial turbulent momentum thickness matched to the laminar value at the experimentally determined transition locations.

An uncertainty existed in the nose-radius history because no instrumentation for measuring surface recession was installed in the nose. Consequently, three nose-radius histories were studied and are shown in figure 4. The nose-radius history of curve ①

was determined from the one-dimensional ablation program of reference 7, considering only the thermochemical oxidation process with equilibrium assumed at the graphite surface. A more realistic prediction, curve (2), was obtained by including the effects of pressure and enthalpy on graphite erosion, as described in reference 8. Curve (3) is a "worst case" radius history initially considered as a possibility because of an anomalous temperature rise in the forward nose-tip thermocouple at approximately 18.288 km (60 000 ft). This history was constructed by assuming a monotonic radius increase to the exposure radius during the period from the beginning of mechanical erosion to the time of the rapid temperature rise.

Based on the minimum and maximum nose-tip-radius histories shown, local flow conditions were computed for an altitude of 30.480 km (100 000 ft) and at 1.524-km (5000-ft) intervals in altitude from 27.432 to 18.288 km (90 000 to 60 000 ft) for 0° angle-of-attack condition. For the present paper, these data were faired (determined to be continuous and smooth) and local flow properties at intermediate altitudes were derived from the resulting curves. The local properties at the beginning and end of transition, based on the minimum and maximum nose radii, are presented in tables I and II, respectively.

Accuracy

The transition locations presented herein are believed to be accurate within ± 0.152 m (± 0.5 ft). Other parameters whose accuracy may be of interest for this paper are the altitude, velocity, and free-stream density. The accuracies of the altitude and velocity are considered to be ± 30.48 m (± 100 ft) and ± 15.24 m/sec (± 50 ft/sec) down to altitudes of approximately 15.240 km (50 000 ft), and the free-stream density is accurate to within 1 percent over the data range.

FLIGHT-TEST RESULTS AND DISCUSSION

Basic Data

The primary experimental data for the flight experiment were the temperatures and pressures measured along the spacecraft. The temperature data and the corresponding heating rates from all 21 sensor stations are presented in reference 2, and the experimental pressure data are presented in reference 3. It should be noted that the experimental pressure data were not used in this paper. Typical temperature histories obtained from the outermost thermocouples at stations 101.6, 215.9, 307.3, and 365.7 cm (40.0, 85.0, 121.0, and 144.0 in.) along $\phi = 0^\circ$ are presented in figure 5.

Transition Data

Heating rates at each thermal measurement station were computed as described in reference 2 from the smoothed temperature histories by a single thermocouple method (ref. 9). A typical heating-rate distribution is presented in figure 6. The beginning and the end of transition are defined herein as the intersection of curves faired through the laminar, transitional, and turbulent heating data, as shown in figure 6. In the preliminary analysis of reference 1, the beginning and the end of transition were approximated from straight lines faired through the laminar, transitional, and turbulent heating data on log-log plots. The location of the beginning and the end of transition from the present technique differed only slightly from the transition locations presented in reference 1.

Faired curves of the heating-rate distributions along the primary ray ($\phi = 0^\circ$) of the body at 0.610-km (2000-ft) intervals in altitude between 32.307 and 18.288 km (106 000 and 60 000 ft) are presented in figure 7. Heating rates are presented for altitudes above 30.480 km (100 000 ft) only so that the altitude at which transition moved onto the vehicle can be approximated. The actual transition locations are difficult to determine above 30.480 km (100 000 ft) and, therefore, no boundary-layer calculations were made above this altitude. The curves are characterized by longitudinally decreasing heating rates in the forward laminar region, sharply increased heating in the transitional zone, and the high level of the turbulent heating over the rearward portion of the spacecraft. With decreasing altitude (increasing dynamic pressure and unit Reynolds number), the forward progression of the beginning and end of transition along the spacecraft is easily observed.

Beginning of transition.- The initial movement of transition onto the spacecraft occurs at an altitude slightly above 30.480 km (100 000 ft). The axial locations of the beginning of boundary-layer transition, as determined from the heating-rate distributions at 0.610-km (2000-ft) intervals for altitudes from 30.480 to 18.288 km (100 000 to 60 000 ft), are listed in table I. These data are presented for the limiting nose-radius conditions previously discussed. The table also provides the laminar local flow properties for the corresponding axial location, altitude, and assumed 0° angle-of-attack condition. The axial locations in table I are shown in figure 8 to illustrate the forward progression of the beginning of boundary-layer transition with decreasing altitude. Also shown in figure 8 are points determined by the temperature-history method discussed later.

End of transition.- The axial locations of the end-of-transition data are given in table II, again at intervals of 0.610 km (2000 ft) in altitude and for the limiting nose-radius conditions. The table includes the turbulent local flow properties (determined as previously discussed) for the corresponding axial location and altitude (assuming zero angle of attack). The forward progression of the turbulent front (end of transition) is

also shown in figure 8. It is noted that the turbulent front lags the beginning of transition by approximately 1.22 m (4 ft) to an altitude of approximately 20.117 km (66 000 ft). Below this altitude the turbulent front appears to remain stationary at station 2.29 m (7.5 ft).

Comparison of Detection Techniques

In recent years, numerous vehicles have been flown with limited thermal instrumentation which was installed primarily for diagnostic purposes; consequently, the thermal instrumentation was insufficient to define the heating-rate distribution along the spacecraft. In these flight experiments, boundary-layer transition was determined by a rapid rise in the temperature-history curve (as described in ref. 10).

For the Reentry F test, the temperature-rise technique is illustrated by the data shown in figure 5 for the primary ray stations 101.6, 215.9, 307.3, and 365.7 cm (40.0, 85.0, 121.0, and 144.0 in.). In figure 5, the time at which the temperature at station 215.9 cm (85.0 in.) experiences a rapid rise is easily detected graphically, but the time of sudden temperature increase for stations 307.3 and 365.7 cm (121.0 and 144.0 in.) is not as well defined.

In order to compare the two transition-determination techniques (transition determined from heating-rate distributions and transition determined from a "knee" in the temperature histories), boundary-layer transition was determined from the temperature histories of the outermost thermocouple (depth approximately 0.0254 cm (0.010 in.)) at the 12 axial locations on the primary ray. It should be noted that there is a negligible difference in the calculated surface temperatures and the outermost thermocouple measurement. The forward movement of transition as determined from the temperature histories is shown in figure 8. The data show that temperature-history-determined transition occurs at a more rearward location at each altitude on the Reentry F spacecraft than does heating-rate-distribution-determined transition. Above 23.470 km (77 000 ft), the temperature-history-determined transition more closely agrees with the end of transition data determined from heating-rate distributions.

Further comparison of the two techniques is presented in figure 9. The heating-rate distributions at altitudes of 29.261, 26.518, 24.384, and 22.555 km (96 000, 87 000, 80 000, and 74 000 ft) are presented, with the beginning of transition as determined from heating-rate distributions and temperature-history techniques noted at each altitude.

From figures 8 and 9, it is obvious that the temperature-history method as currently used for determining transition indicates transition at a more rearward location on the spacecraft than the point where the heating rate departs from the laminar trend. This results in higher transition Reynolds numbers for flight data determined from the temperature-history method, as a result of both the increased length to transition and

the higher local unit Reynolds number at the more rearward stations on slightly blunted cones. Also, the temperature-history method indicates a higher local Mach number at transition for a blunt cone. It is apparent, therefore, that using the rapid rise in the temperature-history curve to indicate the beginning of transition does not provide an accurate substitute for heating-rate distributions when definitive transition studies are being made in flight. Likewise, existing transition Reynolds numbers obtained from flight tests by utilizing the conventional temperature-history technique should not be used in the development of boundary-layer transition correlations for defining the beginning of transition.

It should not be concluded that definitive boundary-layer transition information cannot be obtained from a surface-temperature history provided high-quality data are available. If the first departure from the laminar-theory temperature history is used as the indication of transition (rather than the later sharp upward break), the resulting determination of transition should be in better agreement with the axial location of transition from the heating-rate-distribution method. However, since it is difficult to account accurately for such effects as that of angle of attack in laminar theories, this approach may not always provide a reliable method.

A further improvement in obtaining results from a surface thermocouple measurement can be made by converting the temperature history to a heating-rate history. The heating rate is proportional to the derivative of the temperature-history curve and, therefore, is more sensitive. Typical heating-rate histories from reference 2 are presented in figure 10. As noted by the arrow in the figure, transition is selected as a slight upward break in the data. For the Reentry F flight conditions, this change in slope varies from about 16.9 to 56.5 watts/cm² (15 to 50 Btu/ft²-sec). The sharper break noted in the figure corresponds to the time associated with the "knee" in the temperature-history curve. Transition was determined from the heating-rate histories at each primary thermocouple location, and the results are compared with the results of the heating-rate-distribution method and the conventional temperature-history method in figure 11. The heating-rate-history results are in acceptable agreement with the heating-rate-distribution results.

Effect of Nose Radius on Transition Reynolds Number

Blunting of the nose tip influences the boundary layer for a considerable distance downstream of the blunted nose, and local flow conditions are drastically different from sharp-cone values. Consequently, transition on a blunted cone results in lower transition Reynolds numbers and Mach numbers than those for the sharp cone. Local Reynolds numbers at the beginning of transition are presented as a function of local Mach number in figure 12. The local Reynolds numbers and Mach numbers are shown for the

maximum- and minimum-nose-radius histories of figure 4. With decreasing altitude the transition Reynolds number is noted to increase and then to decrease as blunting effects become predominant. As would be expected, the transition Reynolds numbers based on the minimum-nose-radius history are higher than those based on the maximum-nose-radius history. It should be noted that, for Reentry F, the variation of transition Reynolds number with Mach number (regardless of the nose radius used) can be approximated by a single curve. Wind-tunnel data (refs. 11 and 12) are shown in figure 12 for comparison with the present flight data, and similar trends are noted.

Effect of Angle of Attack on Transition

The symmetry of boundary-layer transition is influenced by the angle of attack of the test vehicle. The angle of attack was less than 1° during the data period. Typical heating-rate distributions on the leeward (primary) and windward (secondary) rays are presented in figure 13 to demonstrate the asymmetry of transition about the body at angle of attack. Although the location of the beginning of transition on the windward ray (secondary ray) cannot be accurately determined because of the wide spacing of the thermal sensors on that ray, it is apparent from the distributions that transition is not symmetrical about the spacecraft.

Another method of observing this asymmetry involves using the point of peak heating (end of transition (ref. 13)). The progression of the point of peak heating on both rays is presented in figure 14. Since the alternate rays ($\phi = 90^\circ$, 180° , and 270°) had insufficient instrumentation to define the heating-rate distribution and subsequently the point of peak heating, the end of transition (peak heating) on these rays was determined from the slope change in the heating-rate history as shown in figure 10. This method is not as accurate as the heating-rate-distribution method. Therefore, the data are presented with estimated accuracy bands only to indicate qualitatively the asymmetry of transition. Several data points for the primary ray are presented for comparative purposes. It is obvious from this figure that the end of transition is not symmetrical about the body. This asymmetry is shown schematically in figure 15, where the spatial distribution of the end of transition is shown in the sketch of the spacecraft for several altitudes.

For the Reentry F spacecraft, transition on the windward side (secondary ray) is observed to be continually farther forward than on the leeward side (primary ray). This result is contrary to most of the wind-tunnel transition data at angle of attack which shows that transition moves farther forward on the leeward side. Most of these tests did not provide data on combined angle of attack and blunting effects and some models were instrumented along only a single ray. However, the phenomena (transition farther forward on the windward ray at angle of attack) was found on a slightly blunted 7.2°

~~CONFIDENTIAL~~

half-angle cone at angles of attack of 1° and 2° (ref. 13), a slender 2.87° half-angle cone at an angle of attack of 2° (ref. 14), and a blunt 25° half-angle cone at an angle of attack of 5° (ref. 15).

CONCLUSIONS

Experimental free-flight transition data have been obtained on a 3.962-m- (13-ft-) long, 5° half-angle cone with an initial nose radius of 0.254 cm (0.10 in.). The data were obtained during reentry from altitudes of about 30.480 to 18.288 km (100 000 to 60 000 ft) at a free-stream Mach number of 20 and a ratio of wall temperature to total temperature near 0.1. During the data period, the free-stream Reynolds number varied from about 6.56×10^6 to 52.5×10^6 per meter (2.0×10^6 to 16.0×10^6 per ft) and the total enthalpy varied from 18.3 to 16.9 MJ/kg (7900 to 7300 Btu/lbm).

The conclusions from the present work are as follows:

1. Transition first occurred on the spacecraft at an altitude slightly above 30.480 km (100 000 ft) and then progressed forward along the spacecraft as the altitude decreased.
2. The temperature-history technique for determining transition as currently used (sharp break in temperature-history curve) compared unfavorably with the heating-rate-distribution method for determining the beginning of transition for the Reentry F experiment.
3. Transition determined from the first slight upward break in the heating-rate-history curve was in better agreement with the heating-rate-distribution results than were the temperature-history results.
4. For the experimental transition-location history a set of computed local transition Reynolds numbers and Mach numbers can be approximated by a single curve regardless of the nose-radius history assumed. The trends of transition observed in the experimental flight data are similar to those observed in wind-tunnel data.
5. Boundary-layer transition was not symmetrical about the body, as indicated by the asymmetry in the location of the peak heating point. For the small angles of attack ($<1.0^\circ$) experienced during reentry, transition was observed to be farther forward on the windward ray than on the leeward ray. This has also been observed in ground tests.

Langley Research Center,
National Aeronautics and Space Administration,
Hampton, Va., April 19, 1971.

REFERENCES

1. Rumsey, Charles B.; Carter, Howard S.; Hastings, Earl C., Jr.; Raper, James L.; and Zoby, Ernest V.: Initial Results From Flight Measurements of Turbulent Heat Transfer and Boundary-Layer Transition at Local Mach Numbers Near 15 (Reentry F). NASA TM X-1856, 1969.
2. Howard, Floyd G.: Thermal Analysis Methods and Basic Heat-Transfer Data for a Turbulent Heating Flight Experiment at Mach 20 (Reentry F). NASA TM X-2282, 1971.
3. Dillon, James L.: Analysis of Surface Pressure on a 5° Cone in Free Flight Near Mach 20 (Reentry F). NASA TM X-2210, 1971.
4. Woodbury, Gerard E.; and Morris, W. Douglas: Angle-of-Attack Analysis of a Spinning Slender Cone With Slight Aerodynamic and Mass Asymmetries (Reentry F). NASA TN D-5948, 1970.
5. Alley, Vernon L., Jr.; and Guillotte, Robert J.: Postflight Analysis of Thermal Distortions of the Reentry F Spacecraft. NASA TM X-2250, 1971.
6. Stainback, P. Calvin (With appendix by P. Calvin Stainback and Kathleen C. Wicker): Effect of Unit Reynolds Number, Nose Bluntness, Angle of Attack, and Roughness on Transition on a 5° Half-Angle Cone at Mach 8. NASA TN D-4961, 1969.
7. Moyer, Carl B.; and Rindal, Roald A.: An Analysis of the Coupled Chemically Reacting Boundary Layer and Charring Ablator. Part II. Finite Difference Solution for the In-Depth Response of Charring Materials Considering Surface Chemical and Energy Balances. NASA CR-1061, 1968.
8. Kratsch, K. M.; Martinez, M. R.; Clayton, F. I.; Greene, R. B.; and Wuerer, J. E.: Graphite Ablation in High-Pressure Environments. AIAA Paper No. 68-1153, Dec. 1968.
9. Howard, Floyd G.: Single-Thermocouple Method for Determining Heat Flux to a Thermally Thick Wall. NASA TN D-4737, 1968.
10. Sherman, M. M.; and Nakamura, T.: Flight Test Measurements of Boundary Layer Transition on a Non-Ablating 22-Degree Cone. AIAA Paper No. 68-1152, Dec. 1968.
11. Stetson, Kenneth F.; and Rushton, George H.: A Shock Tunnel Investigation of the Effects of Nose Bluntness, Angle of Attack and Boundary Layer Cooling on Boundary Layer Transition at a Mach Number of 5.5. AIAA Paper No. 66-495, June 1966.

- ~~CONFIDENTIAL~~
12. Softly, Eric J.: Boundary Layer Transition on Hypersonic Blunt, Slender Cones. AIAA Paper No. 69-705, June 1969.
 13. Martellucci, A.; and Neff, R. S.: The Influence of Asymmetric Transition on Re-Entry Vehicle Motion. AIAA Paper No. 70-987, Aug. 1970.
 14. Maddalon, Dal V.; and Henderson, Arthur, Jr.: Hypersonic Transition Studies on a Slender Cone at Small Angles of Attack. AIAA J., vol. 6, no. 1, Jan. 1968, pp. 176-177.
 15. Bushnell, Dennis M.; Jones, Robert A.; and Huffman, Jarrett K.: Heat-Transfer and Pressure Distributions on Spherically Blunted 25° Half-Angle Cone at Mach 8 and Angles of Attack up to 90° . NASA TN D-4792, 1968.

TABLE I.- TEST CONDITIONS AT BEGINNING OF TRANSITION

h		r		x		Re,x	Me	Hw He	δ*		θ	
km	ft	cm	in.	m	ft				cm	in.	cm	in.
Small nose radius												
30.480	100 000	0.3149	0.124	2.926	9.6	43.5 × 10 ⁶	15.11	1.01	3.111 × 10 ⁻²	1.225 × 10 ⁻²	9.957 × 10 ⁻⁴	3.92 × 10 ⁻⁴
29.870	98 000	.3200	.126	2.835	9.3	46.0	15.09	1.00	2.896	1.14	9.271	3.65
29.261	96 000	.3226	.127	2.743	9.0	48.5	15.05	.99	2.718	1.07	8.636	3.40
28.651	94 000	.3277	.129	2.438	8.0	47.0	14.99	.98	2.535	.998	8.052	3.17
28.042	92 000	.3302	.130	2.377	7.8	49.5	14.95	.98	2.375	.935	7.544	2.97
27.432	90 000	.3353	.132	2.316	7.6	54.0	14.91	.97	2.230	.878	7.036	2.77
26.822	88 000	.3391	.1335	2.256	7.4	56.5	14.83	.98	2.121	.835	6.655	2.62
26.213	86 000	.3429	.135	2.225	7.3	60.5	14.74	.98	1.999	.787	6.350	2.50
25.908	85 000	.3467	.1365	2.195	7.2	62.0	14.74	.98	1.943	.765	6.172	2.43
25.603	84 000	.3480	.137	2.164	7.1	63.0	14.62	.98	1.877	.739	6.045	2.38
24.994	82 000	.3531	.139	2.073	6.8	64.0	14.52	.98	1.753	.690	5.715	2.25
24.384	80 000	.3581	.141	2.012	6.6	68.0	14.43	.98	1.626	.640	5.461	2.15
23.774	78 000	.3632	.143	1.676	5.5	58.0	13.99	1.00	1.440	.567	5.080	2.00
23.165	76 000	.3683	.145	1.615	5.3	57.0	13.75	1.01	1.260	.496	4.801	1.89
22.860	75 000	.3721	.1465	1.433	4.7	49.0	13.41	1.02	1.176	.463	4.623	1.82
22.555	74 000	.3747	.1475	1.402	4.6	47.0	13.23	1.04	1.118	.440	4.521	1.78
21.946	72 000	.3810	.150	1.341	4.4	47.5	12.94	1.09	1.008	.397	4.394	1.73
21.336	70 000	.3861	.152	1.219	4.0	41.5	12.40	1.13	.904	.356	4.318	1.70
20.726	68 000	.3937	.155	.930	3.05	22.5	11.00	1.20	.777	.306	4.318	1.70
20.117	66 000	.3988	.157	.872	2.86	19.5	10.40	1.40	.650	.256	4.394	1.73
19.812	65 000	.4013	.158	.853	2.8	19.0	10.20	1.54	.584	.230	4.496	1.77
19.507	64 000	.4064	.160	.808	2.65	16.5	9.70	1.84	.513	.202	4.902	1.93
18.898	62 000	.4140	.163	.686	2.25	10.5	8.75	2.65	.386	.152	5.944	2.34
18.288	60 000	.4204	.1655	.427	1.40	2.2	6.17	3.80	.277	.109	7.569	2.98
Large nose radius												
30.480	100 000	0.3150	0.124	2.926	9.6	43.5 × 10 ⁶	15.11	1.01	3.111 × 10 ⁻²	1.225 × 10 ⁻²	9.957 × 10 ⁻⁴	3.92 × 10 ⁻⁴
29.870	98 000	.3200	.126	2.835	9.3	46.5	15.09	1.00	2.921	1.15	9.322	3.67
29.261	96 000	.3277	.129	2.743	9.0	48.5	15.02	1.00	2.743	1.08	8.738	3.44
28.651	94 000	.3404	.134	2.438	8.0	46.0	14.90	1.00	2.548	1.003	8.230	3.24
28.042	92 000	.3569	.1405	2.377	7.8	48.0	14.80	1.00	2.433	.958	7.747	3.05
27.432	90 000	.3734	.147	2.316	7.6	51.0	14.70	1.00	2.250	.886	7.239	2.85
26.882	88 000	.3886	.153	2.256	7.4	54.0	14.52	1.01	2.113	.832	6.858	2.70
26.213	86 000	.4089	.161	2.225	7.3	56.0	14.37	1.015	1.976	.778	6.604	2.60
25.908	85 000	.4178	.1645	2.195	7.2	57.4	14.29	1.02	1.892	.745	6.477	2.55
25.603	84 000	.4280	.1685	2.164	7.1	57.0	14.13	1.03	1.849	.728	6.299	2.48
24.994	82 000	.4496	.177	2.073	6.8	57.0	13.85	1.05	1.715	.675	6.096	2.40
24.384	80 000	.4775	.188	2.012	6.6	57.0	13.6	1.08	1.588	.625	6.045	2.38
23.774	78 000	.5080	.200	1.676	5.5	39.5	12.53	1.22	1.372	.540	6.147	2.42
23.165	76 000	.5436	.214	1.615	5.3	34.0	11.83	1.45	1.130	.445	6.477	2.55
22.860	75 000	.5613	.221	1.433	4.7	24.5	11.04	1.575	1.019	.401	6.731	2.65
22.555	74 000	.5817	.229	1.402	4.6	22.0	10.58	1.75	.953	.375	7.010	2.76
21.946	72 000	.6172	.243	1.341	4.4	17.2	9.6	2.08	.826	.325	7.874	3.10
21.336	70 000	.6731	.265	1.219	4.0	11.0	8.4	2.60	.706	.278	8.992	3.54
20.726	68 000	.7290	.287	.930	3.05	3.85	6.5	3.65	.577	.227	11.430	4.50
20.117	66 000	.7874	.310	.872	2.86	2.6	5.75	5.1	.465	.183	14.732	5.80
19.812	65 000	.8179	.322	.853	2.8	2.33	5.5	5.96	.422	.166	16.129	6.35
19.507	64 000	.8687	.342	.808	2.65	1.90	5.22	6.68	.399	.157	17.399	6.85
18.898	62 000	.9169	.361	.686	2.25	1.25	4.70	8.25	.361	.142	19.126	7.53
18.288	60 000	.9881	.389	.427	1.40	.61	4.15	9.85	.3366	.1325	20.650	8.13

TABLE II.- TEST CONDITIONS AT END OF TRANSITION

h		r		x		Re,x	Me	Hw He	δ*		θ	
km	ft	cm	in.	m	ft				cm	in.	cm	in.
Small nose radius												
25.603	84 000	0.3480	0.137	3.353	11.0	98 × 10 ⁶	14.69	0.695	7.137 × 10 ⁻²	2.81 × 10 ⁻²	22.860 × 10 ⁻⁴	9.0 × 10 ⁻⁴
24.994	82 000	.3531	.139	3.231	10.6	105	14.7	.71	7.163	2.82	22.301	8.78
24.384	80 000	.3581	.141	3.139	10.3	111	14.7	.74	7.188	2.83	22.962	9.04
23.774	78 000	.3632	.143	2.957	9.7	116	14.74	.75	6.502	2.56	21.082	8.3
23.165	76 000	.3683	.145	2.835	9.3	124	14.75	.73	6.058	2.385	19.812	7.8
22.860	75 000	.3721	.1465	2.652	8.7	125	14.91	.72	5.410	2.13	17.780	7.0
22.555	74 000	.3747	.1475	2.560	8.4	132	15.00	.70	5.144	2.025	16.942	6.67
21.946	72 000	.3810	.150	2.499	8.2	142	15.00	.665	5.144	2.025	17.577	6.92
21.336	70 000	.3861	.152	2.408	7.9	150	14.97	.625	5.156	2.03	17.374	6.84
20.726	68 000	.3937	.155	2.316	7.6	162	15.01	.595	5.207	2.05	16.688	6.57
20.117	66 000	.3988	.157	2.286	7.5	178	15.00	.565	5.512	2.17	16.485	6.49
19.812	65 000	.4013	.158	2.286	7.5	188	15.01	.55	5.639	2.22	16.447	6.475
19.507	64 000	.4064	.160	2.286	7.5	198	15.05	.53	5.817	2.29	16.383	6.45
18.898	62 000	.4140	.163	2.286	7.5	218	15.10	.50	6.121	2.41	16.180	6.37
18.288	60 000	.4204	.1655	2.286	7.5	241	15.15	.46	6.401	2.52	15.939	6.275
Large nose radius												
25.603	84 000	0.4280	0.1685	3.353	11.0	107 × 10 ⁶	14.98	0.71	6.883 × 10 ⁻²	2.71 × 10 ⁻²	21.234 × 10 ⁻⁴	8.36 × 10 ⁻⁴
24.994	82 000	.4496	.177	3.231	10.6	115	15.11	.70	6.071	2.39	18.644	7.34
24.384	80 000	.4775	.188	3.139	10.3	125	15.17	.71	5.436	2.14	16.510	6.50
23.774	78 000	.5080	.200	2.957	9.7	128	15.16	.71	5.207	2.05	17.399	6.85
23.165	76 000	.5436	.214	2.835	9.3	132	15.12	.70	5.652	2.225	21.844	8.60
22.860	75 000	.5613	.221	2.652	8.7	130	15.08	.70	5.512	2.17	22.200	8.74
22.555	74 000	.5817	.229	2.560	8.4	128	14.98	.70	5.029	1.98	19.685	7.75
21.946	72 000	.6172	.243	2.499	8.2	134	14.81	.675	4.343	1.71	16.066	6.325
21.336	70 000	.6731	.265	2.408	7.9	141	14.70	.65	3.835	1.51	13.208	5.20
20.726	68 000	.7290	.287	2.316	7.6	149	14.69	.625	4.115	1.62	14.732	5.80
20.117	66 000	.7874	.310	2.286	7.5	165	14.70	.58	5.436	2.14	17.209	6.775
19.812	65 000	.8179	.322	2.286	7.5	175	14.77	.55	6.121	2.41	18.415	7.25
19.507	64 000	.8687	.342	2.286	7.5	185	14.78	.54	6.401	2.52	18.567	7.31
18.898	62 000	.9169	.361	2.286	7.5	209	14.79	.50	6.883	2.71	18.720	7.37
18.288	60 000	.9881	.389	2.286	7.5	233	14.80	.49	7.290	2.87	16.840	6.63

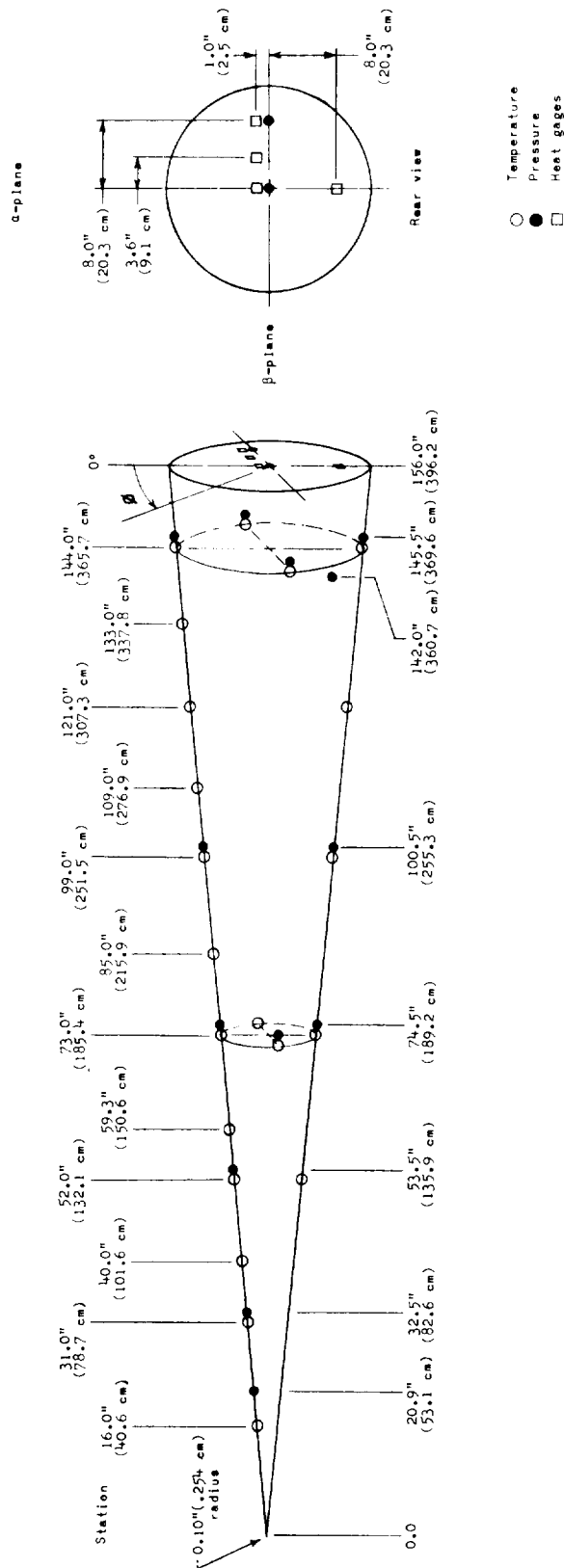
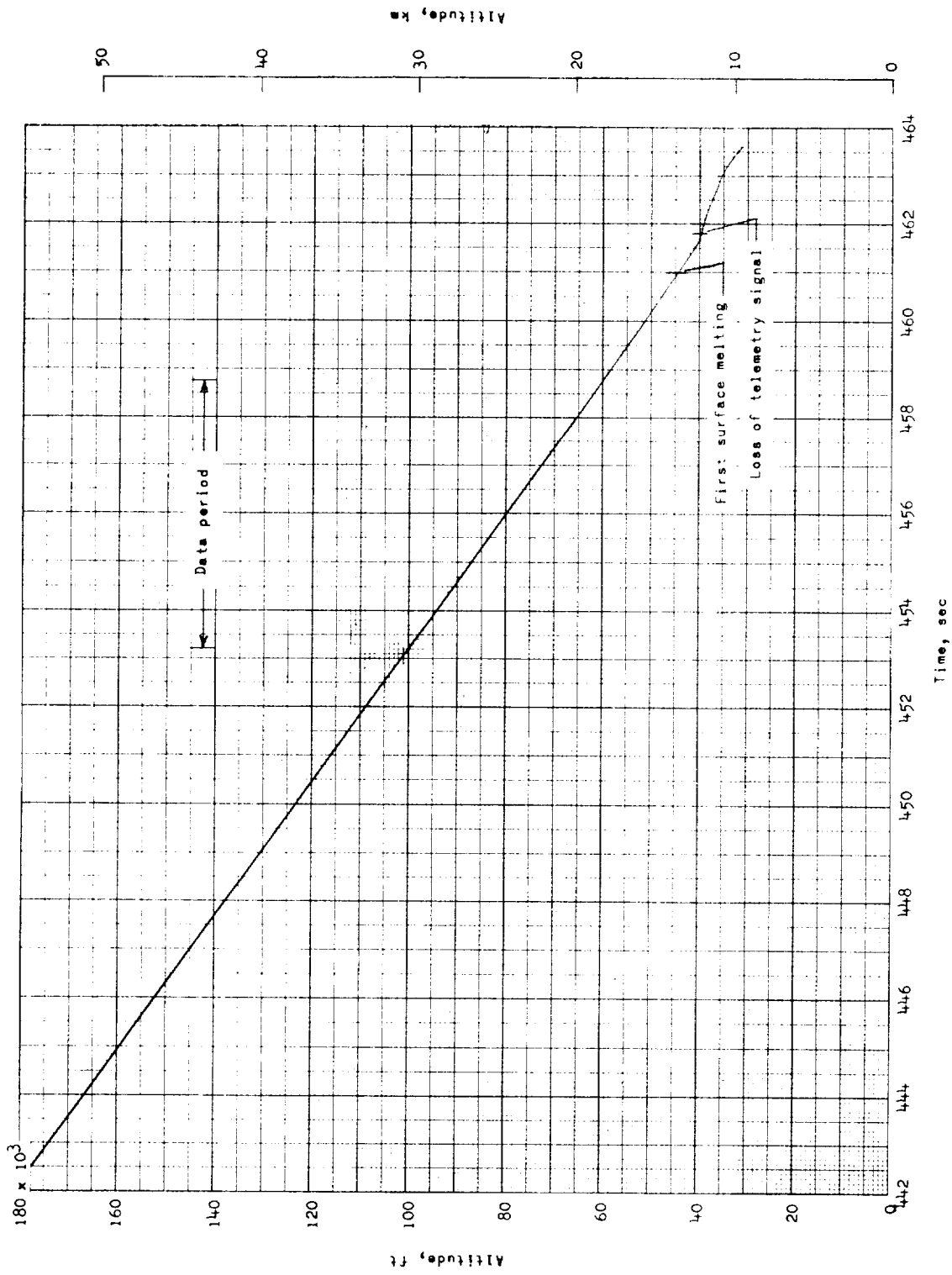
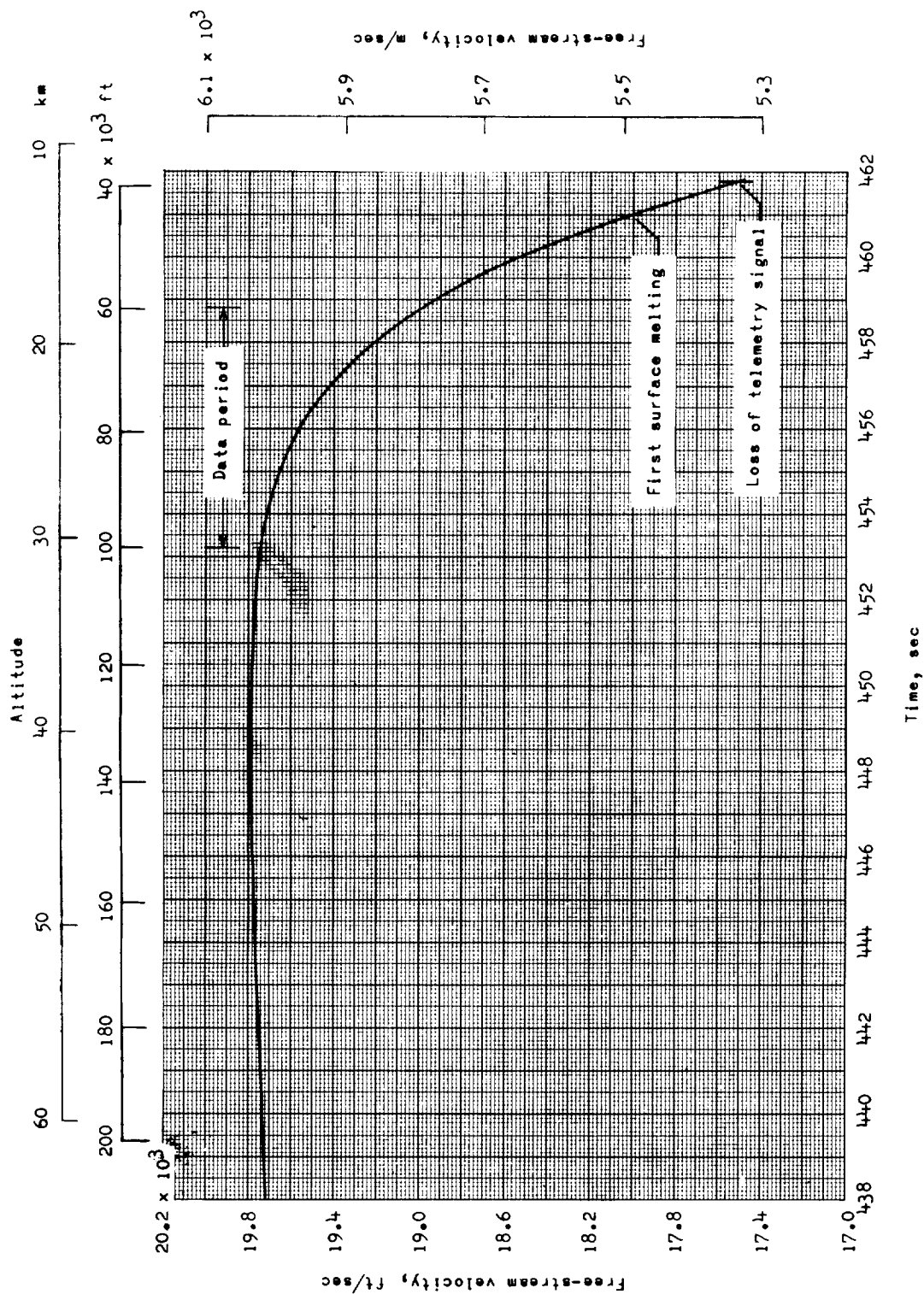


Figure 1.- Axial station locations of temperature and pressure measurements.



(a) Altitude.

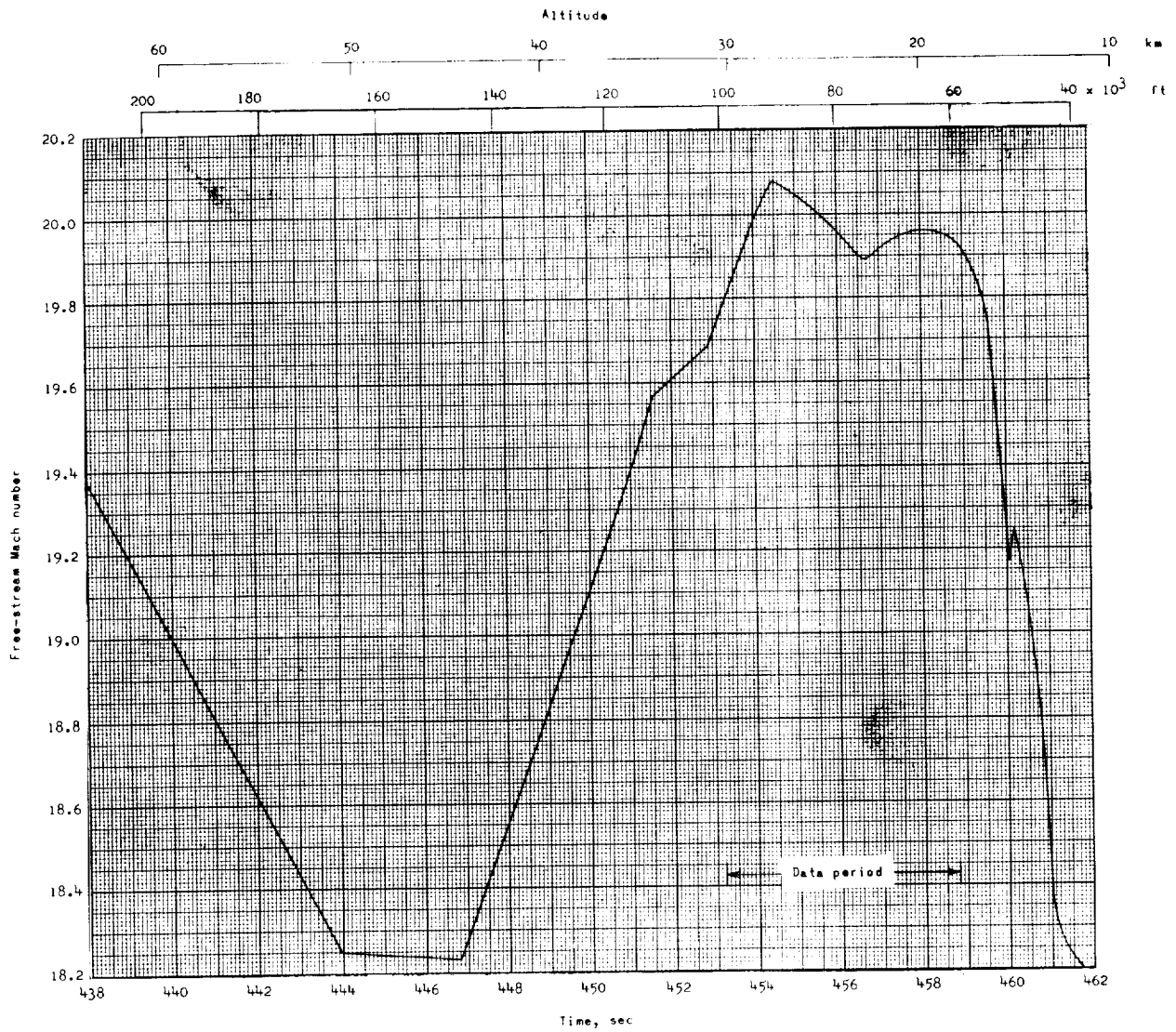
Figure 2.- Histories of free-stream conditions during reentry.



(b) Velocity.

Figure 2.- Continued.

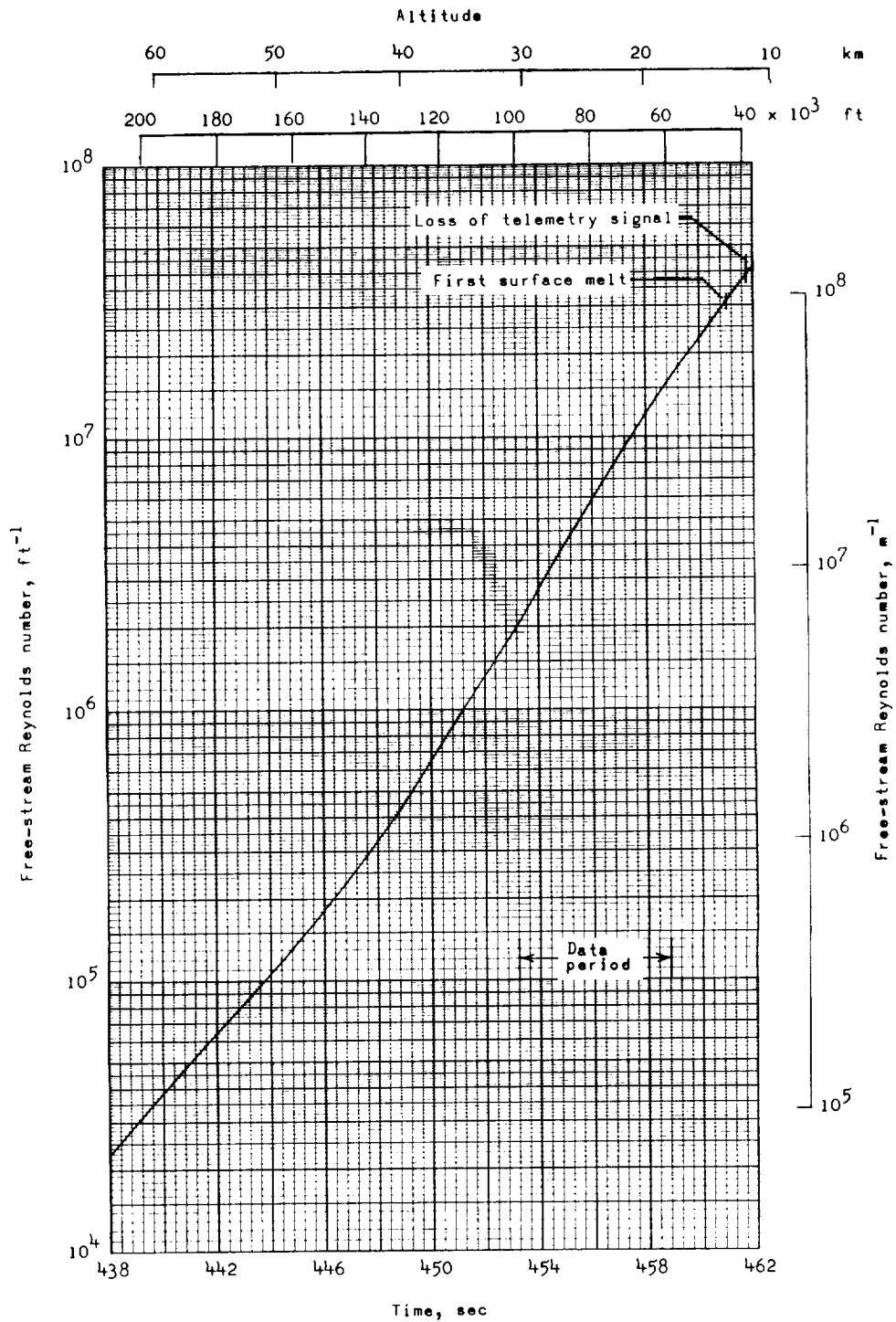
~~CONFIDENTIAL~~



(c) Mach number.

Figure 2.- Continued.

~~CONFIDENTIAL~~



(d) Unit Reynolds number.

Figure 2.- Concluded.

~~CONFIDENTIAL~~

~~CONFIDENTIAL~~

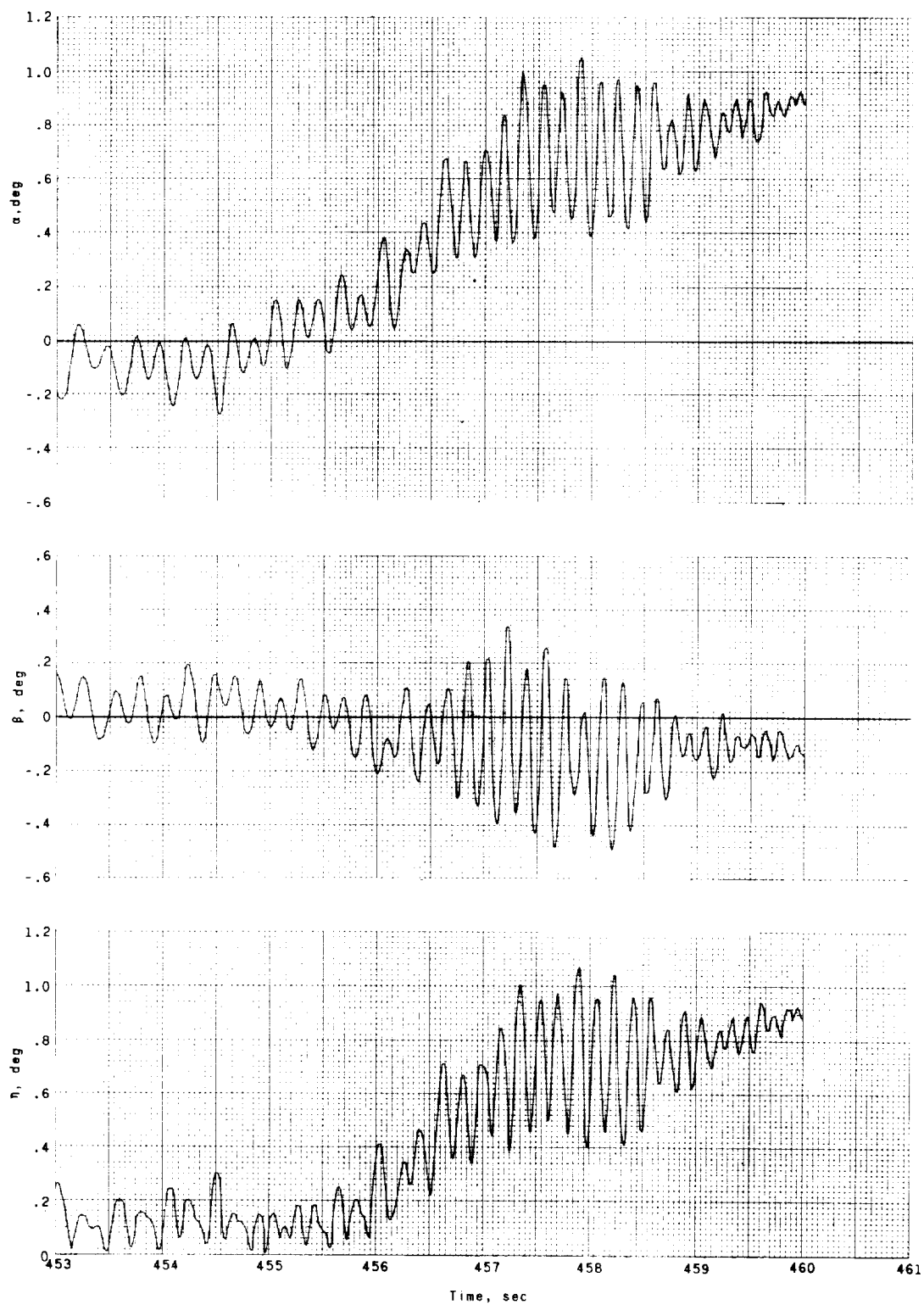
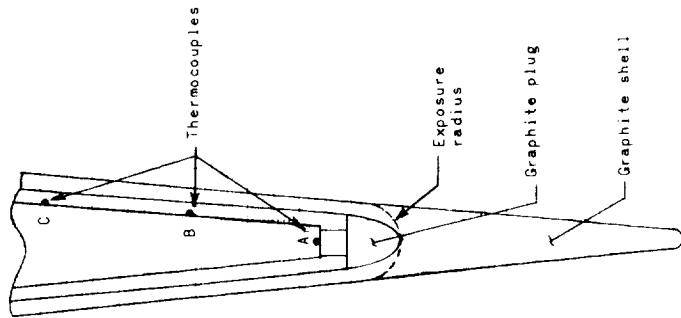
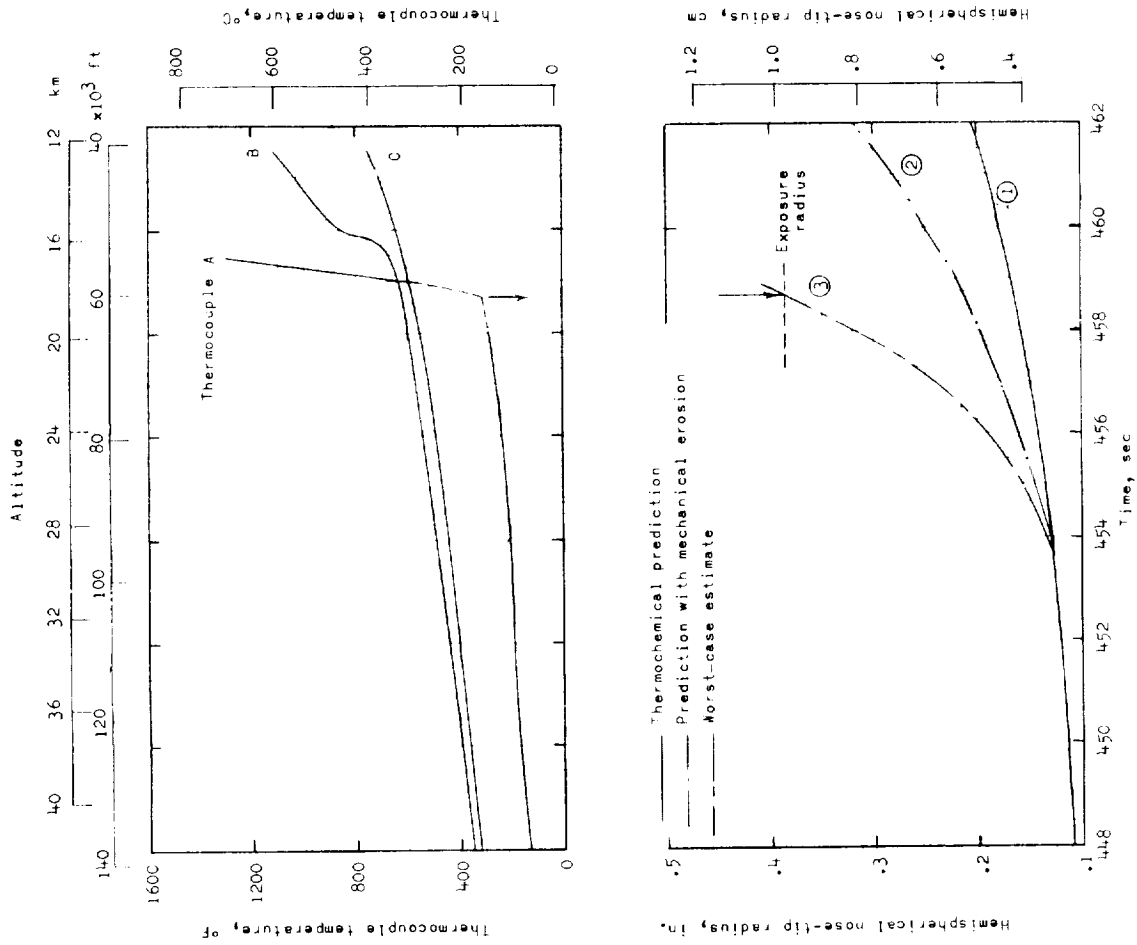


Figure 3.- Body motions in thermal axis system.

~~CONFIDENTIAL~~

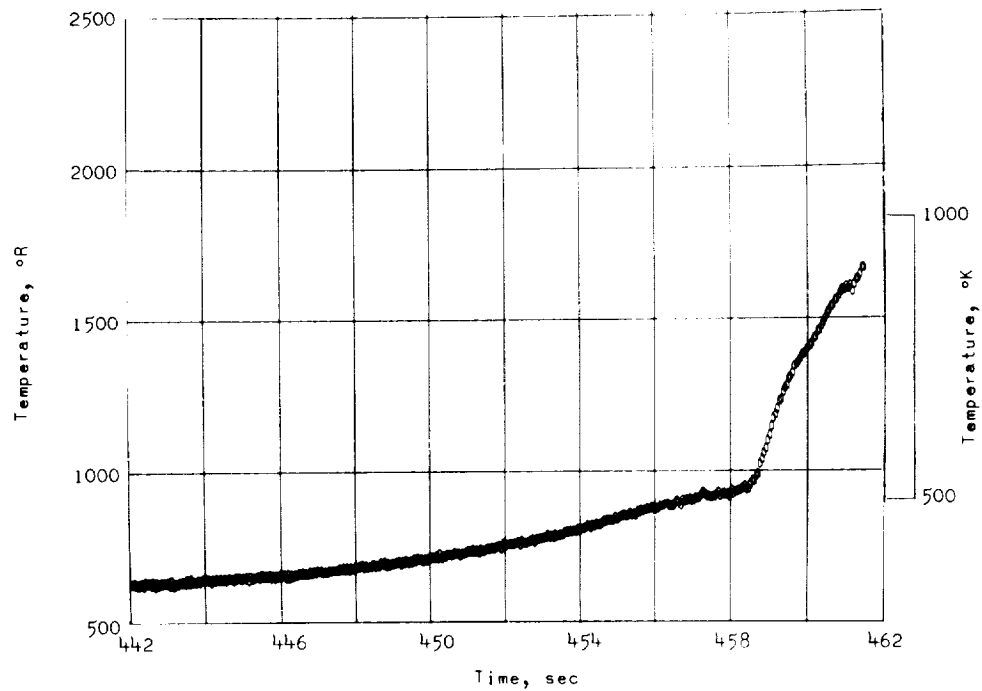


(a) Schematic.

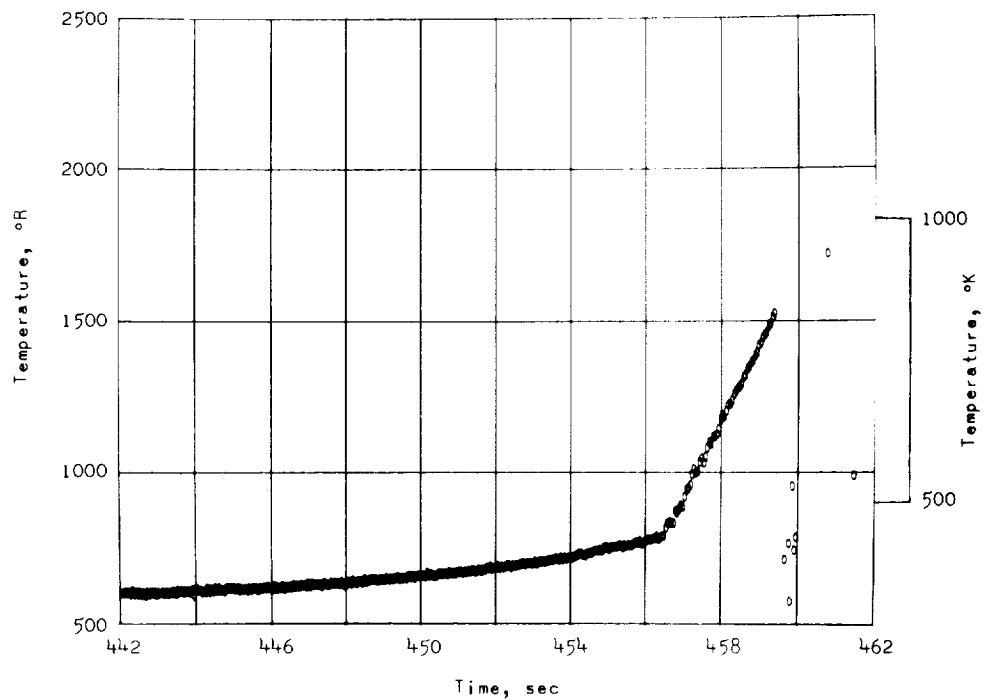


(b) Measured temperatures and recession estimates.

Figure 4.- Nose-tip recession performance.

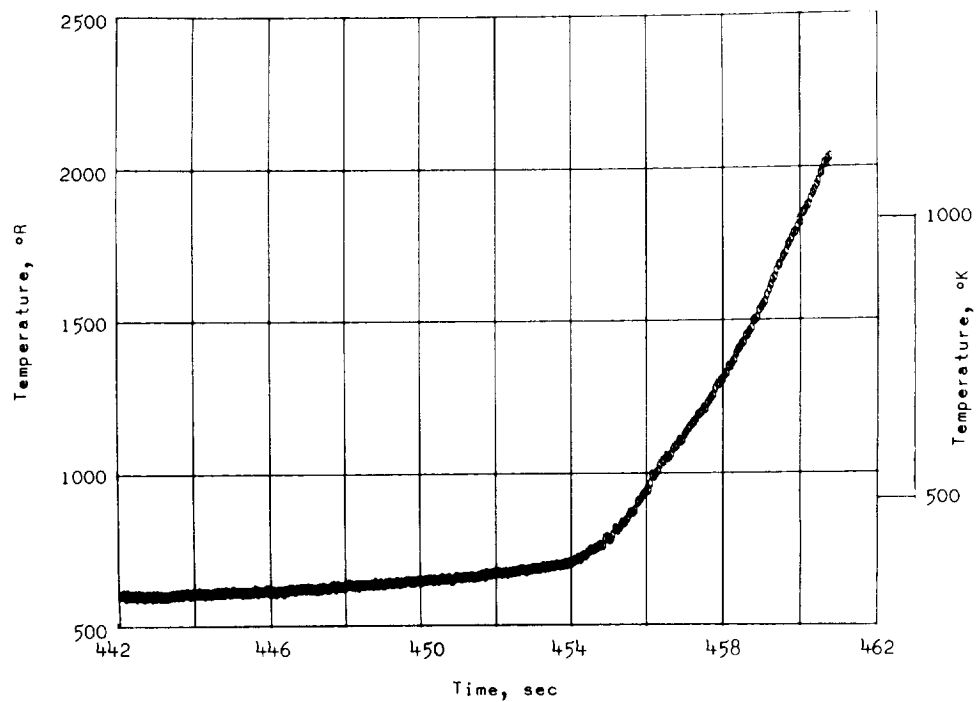


(a) Station 101.6 cm (40.0 in.).

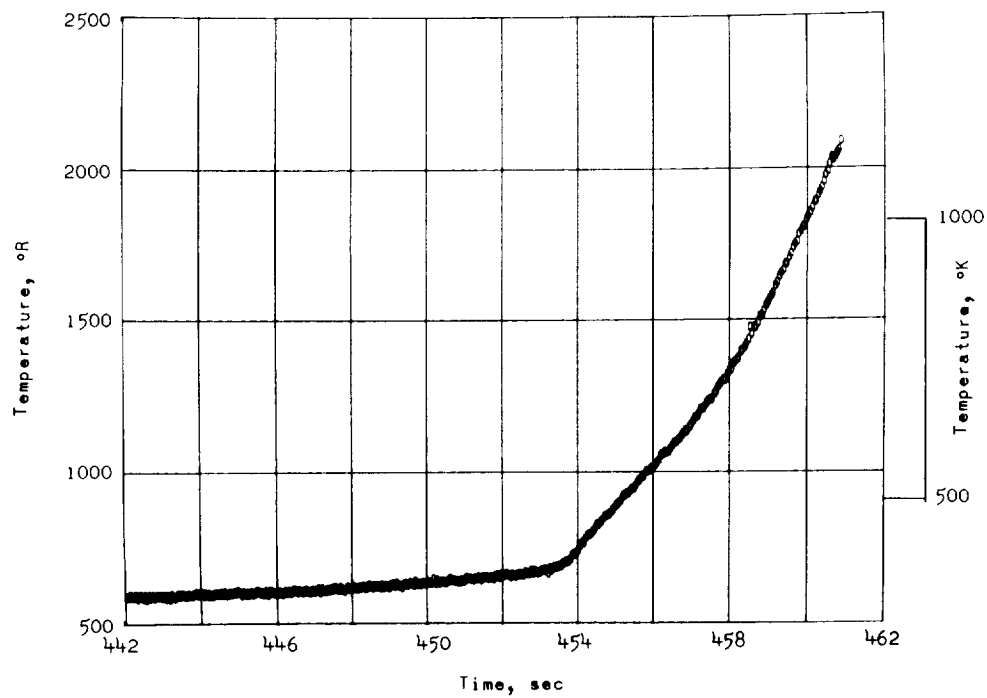


(b) Station 215.9 cm (85.0 in.).

Figure 5.- Typical temperature histories of near-surface thermocouples ($\phi = 0^\circ$).



(c) Station 307.3 cm (121.0 in.).



(d) Station 365.7 cm (144.0 in.).

Figure 5.- Concluded.

~~CONFIDENTIAL~~

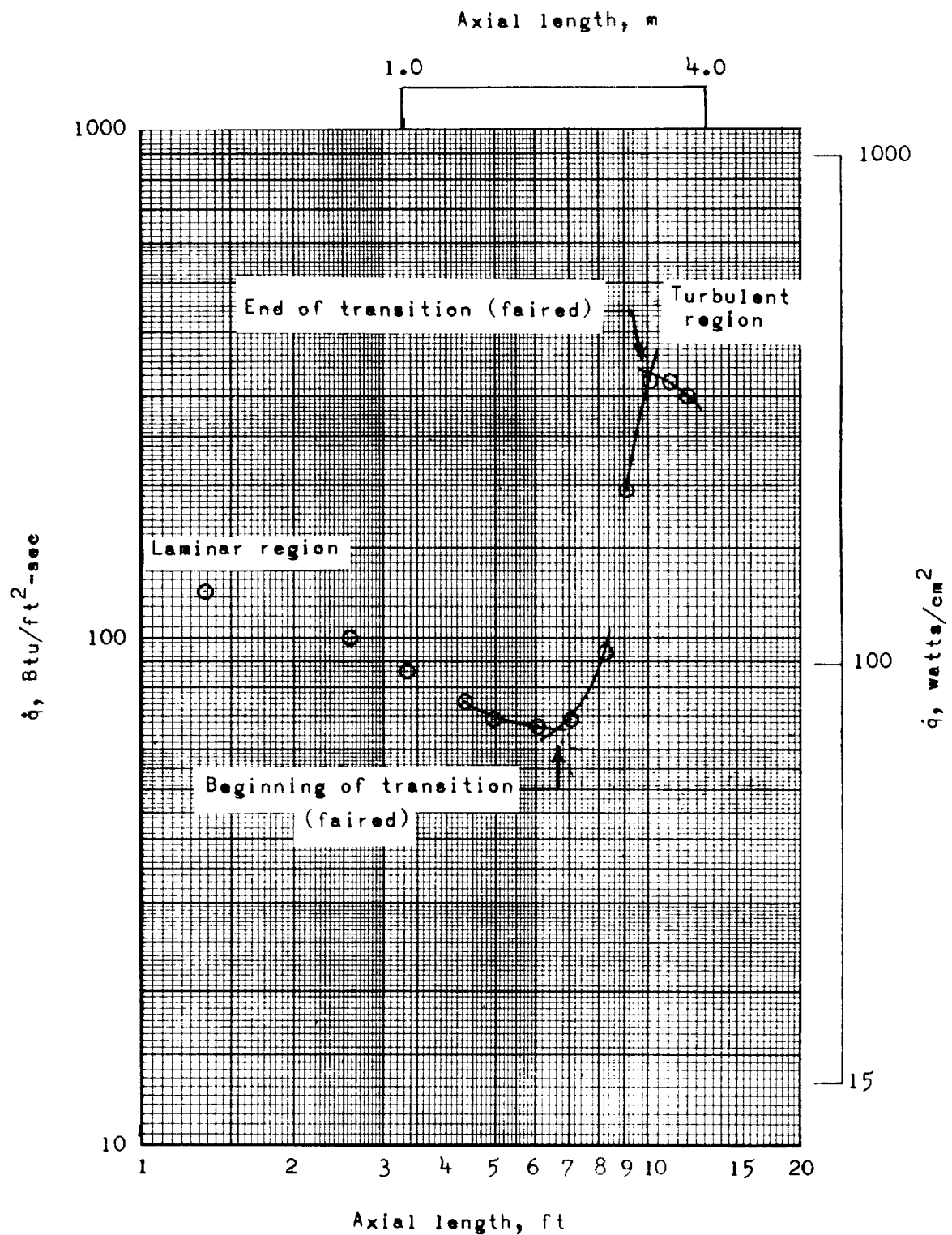
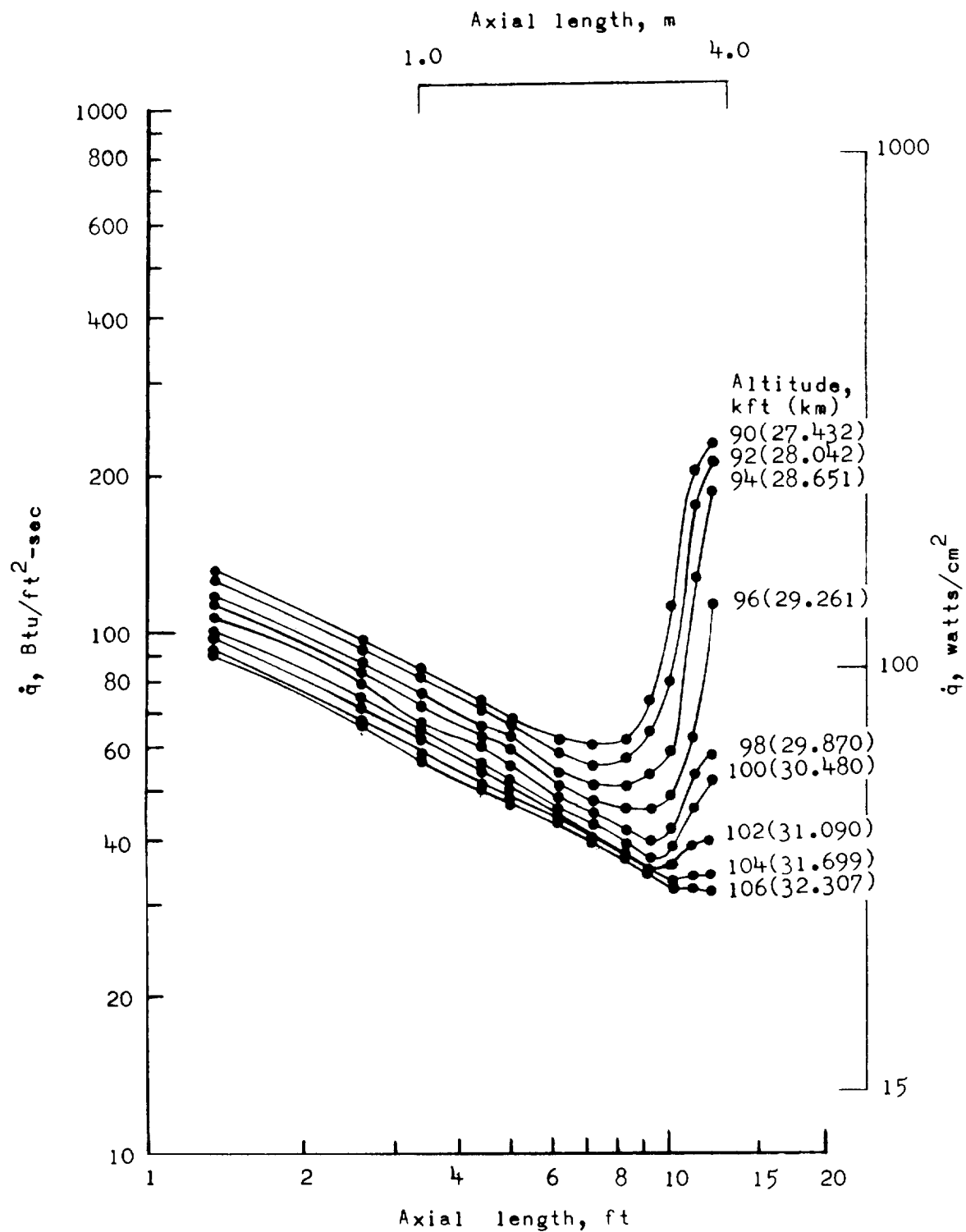


Figure 6.- Determination of transition from typical heating-rate distribution for altitude of 24.384 km (80 000 ft).

~~CONFIDENTIAL~~



(a) Altitudes from 32.307 to 27.432 km (106 000 to 90 000 ft).

Figure 7.- Heating-rate distributions over altitude range from 32.307 to 18.288 km
(106 000 to 60 000 ft).

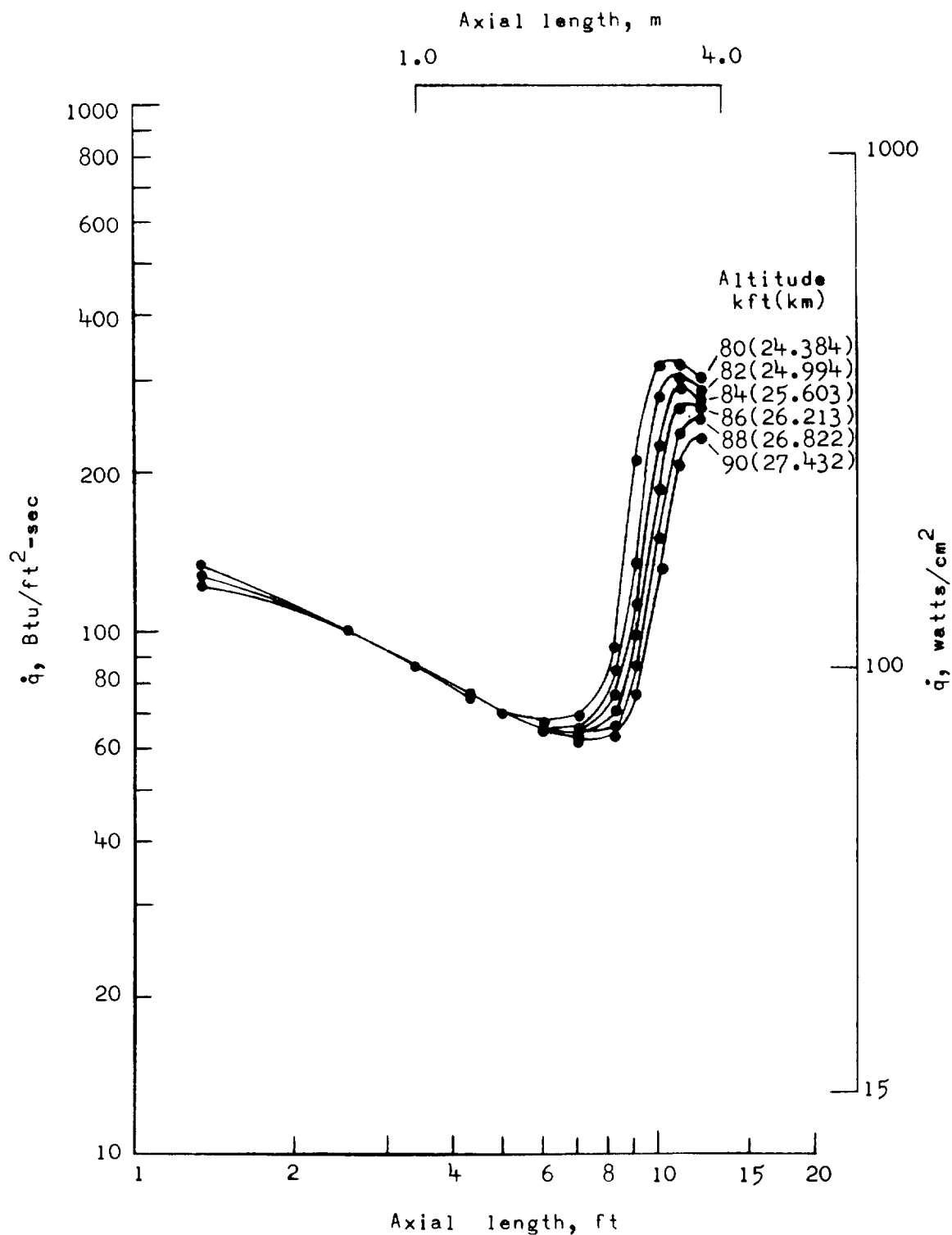
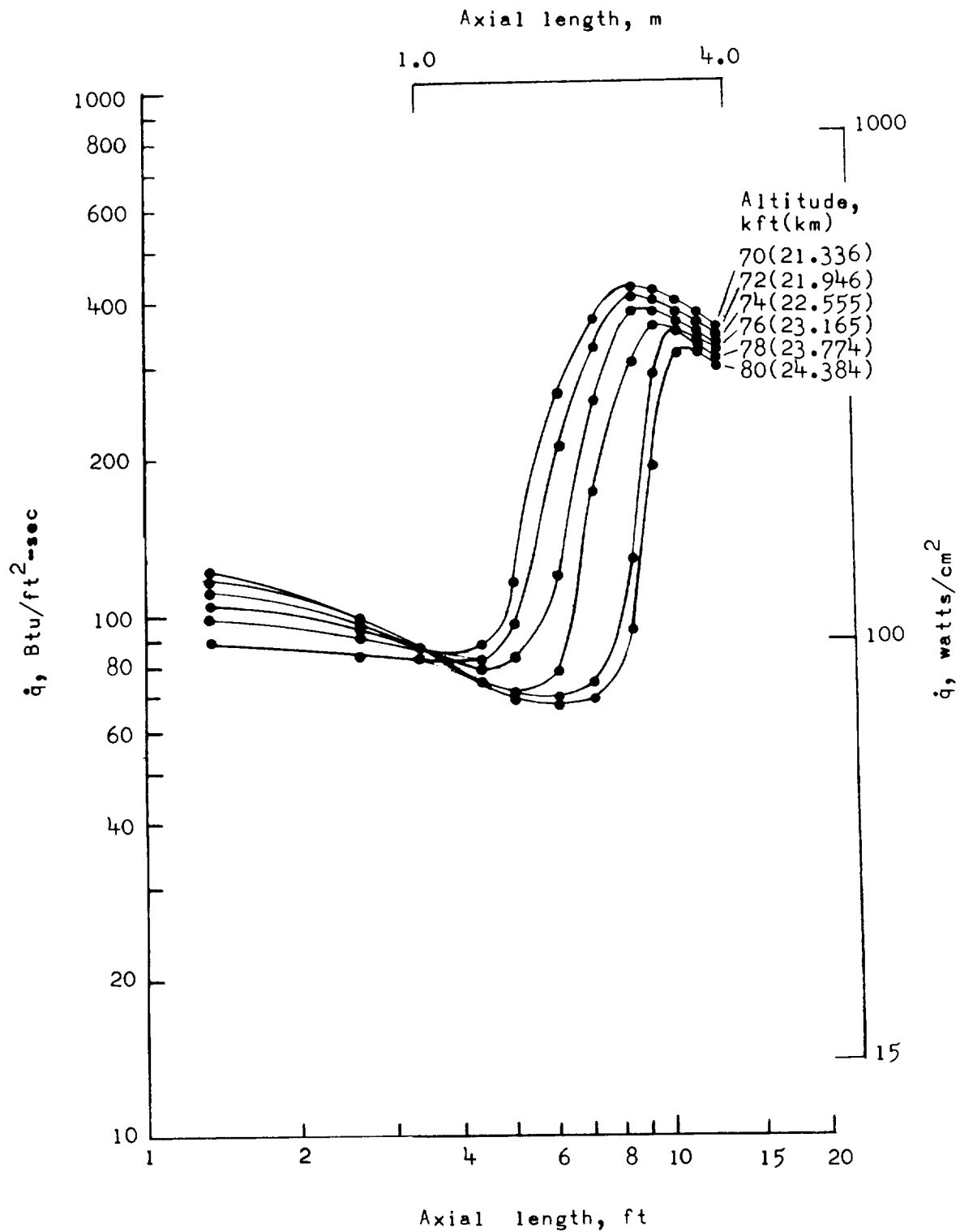
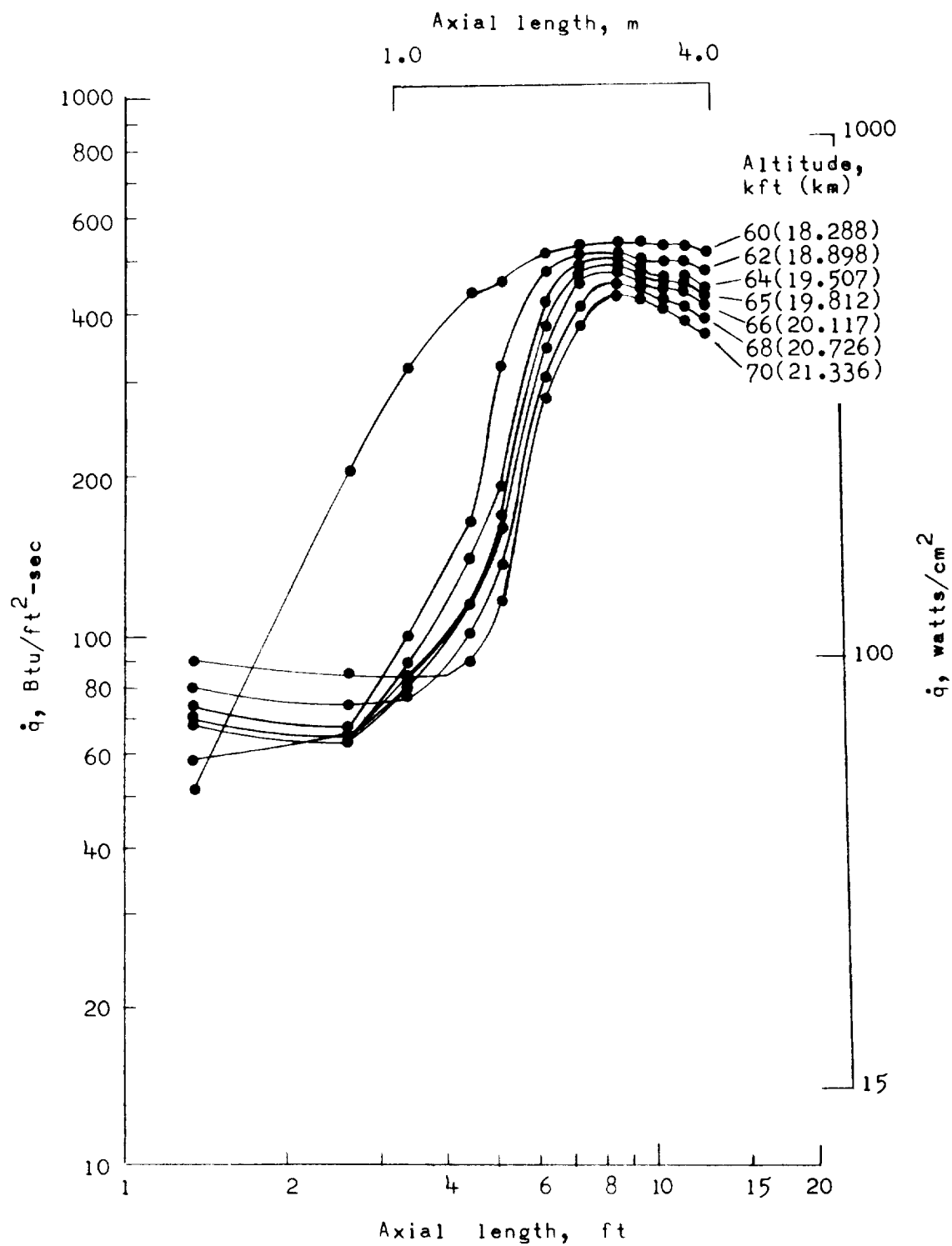


Figure 7.- Continued.



(c) Altitudes from 24.384 to 21.336 km (80 000 to 70 000 ft).

Figure 7.- Continued.



(d) Altitudes from 21.336 to 12.288 km (70 000 to 60 000 ft).

Figure 7.- Concluded.

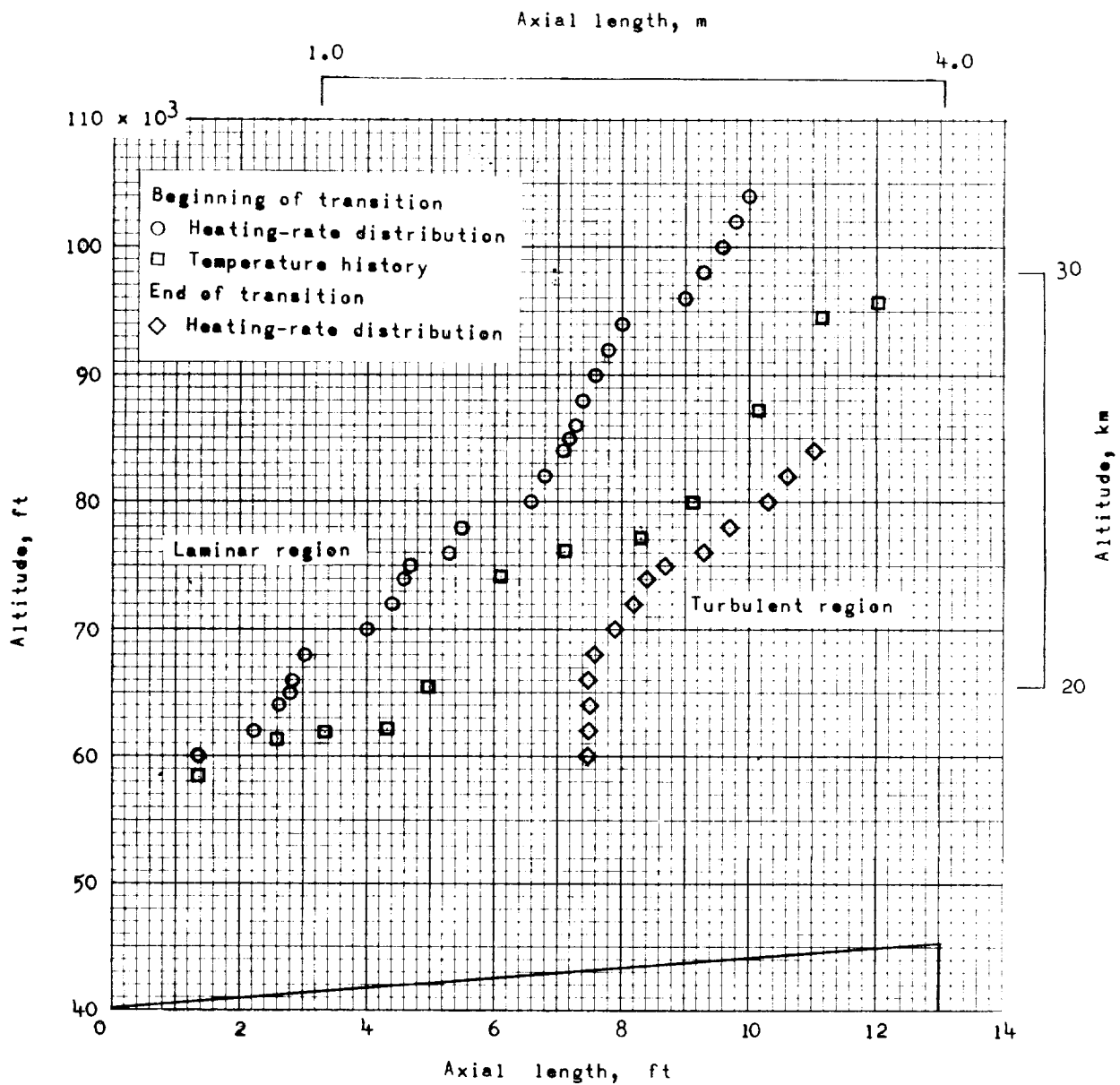


Figure 8.- Axial distributions of beginning and end of transition.

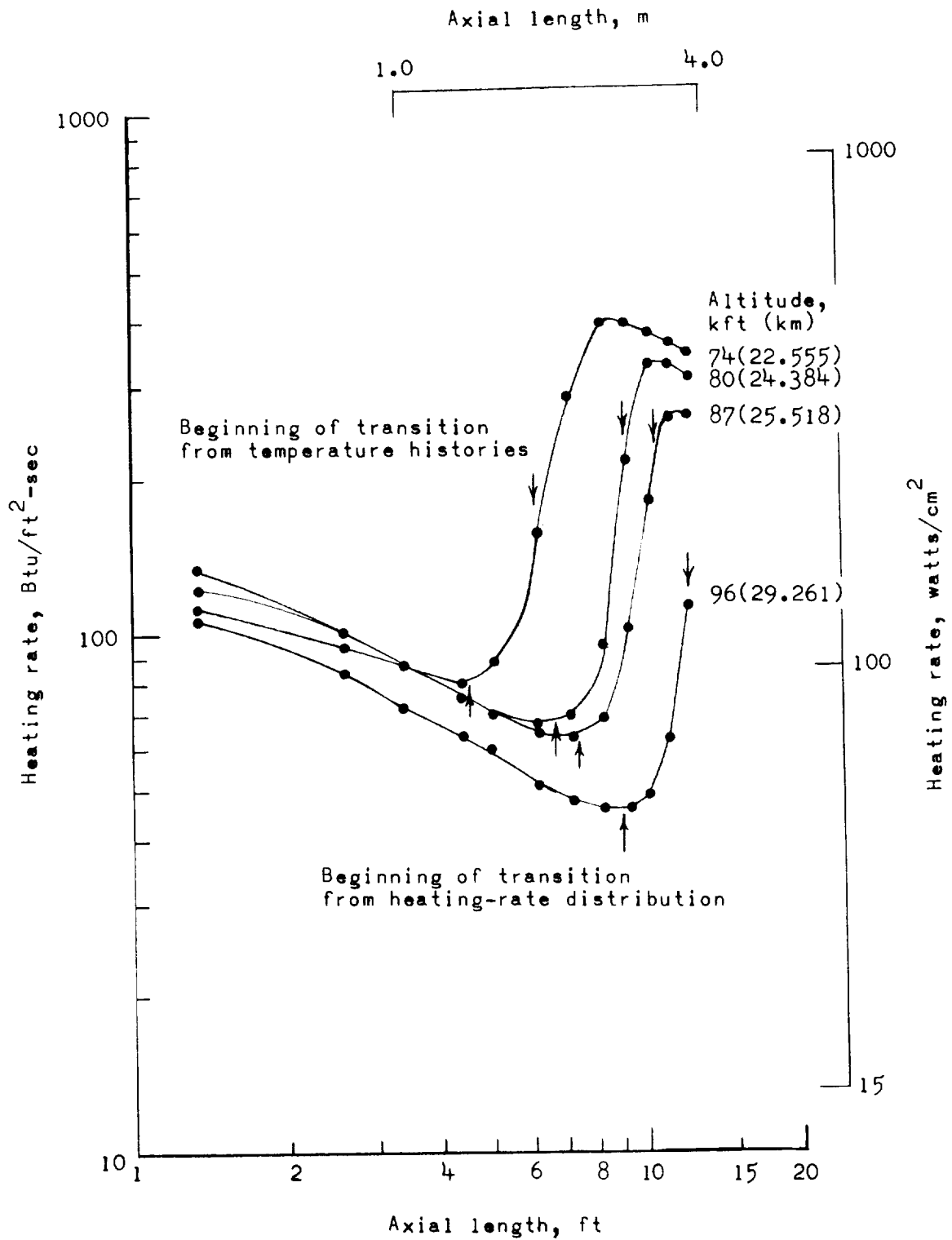
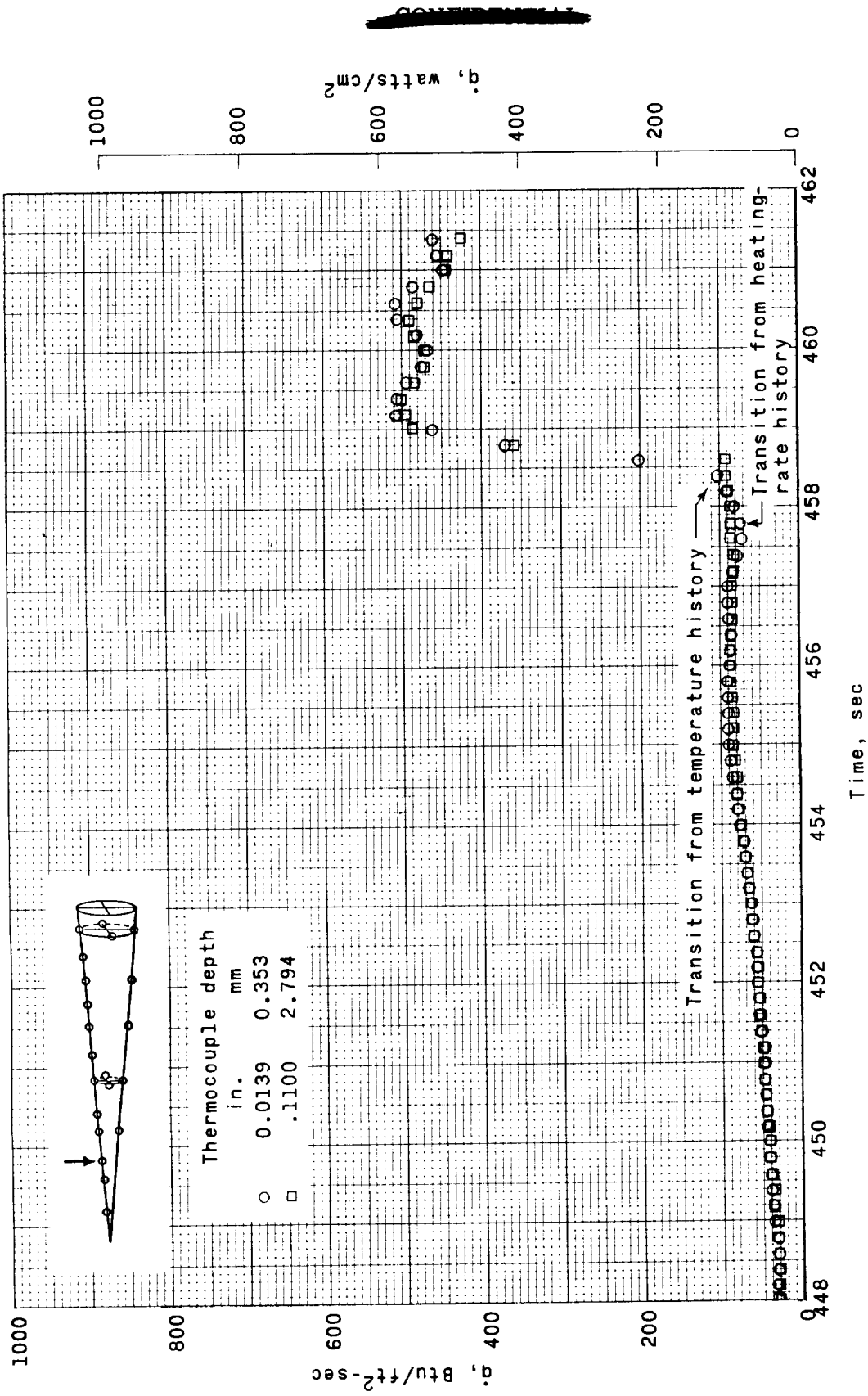
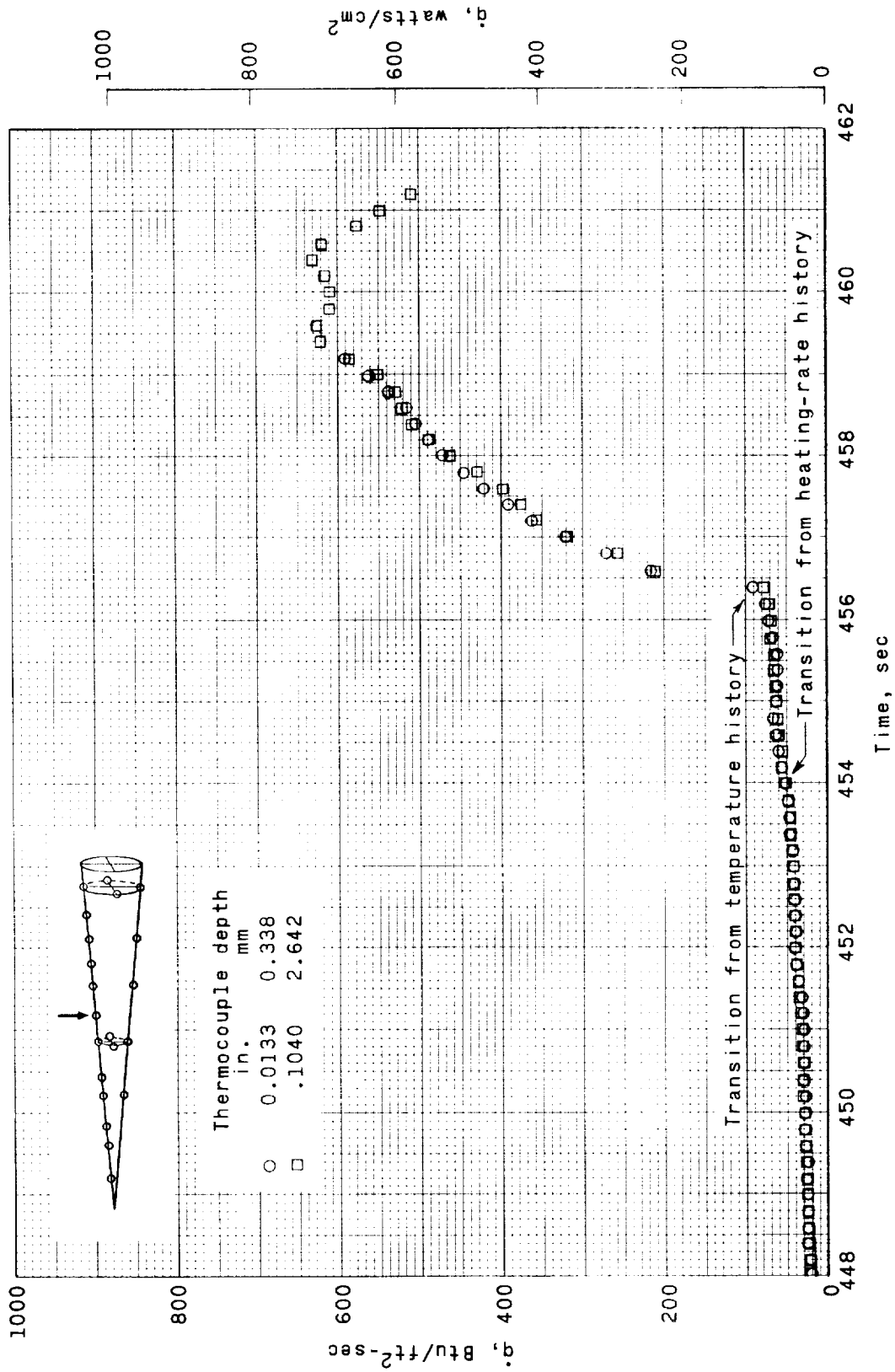


Figure 9.- Comparison of transition locations from heating-rate-distribution and temperature-history determination methods.



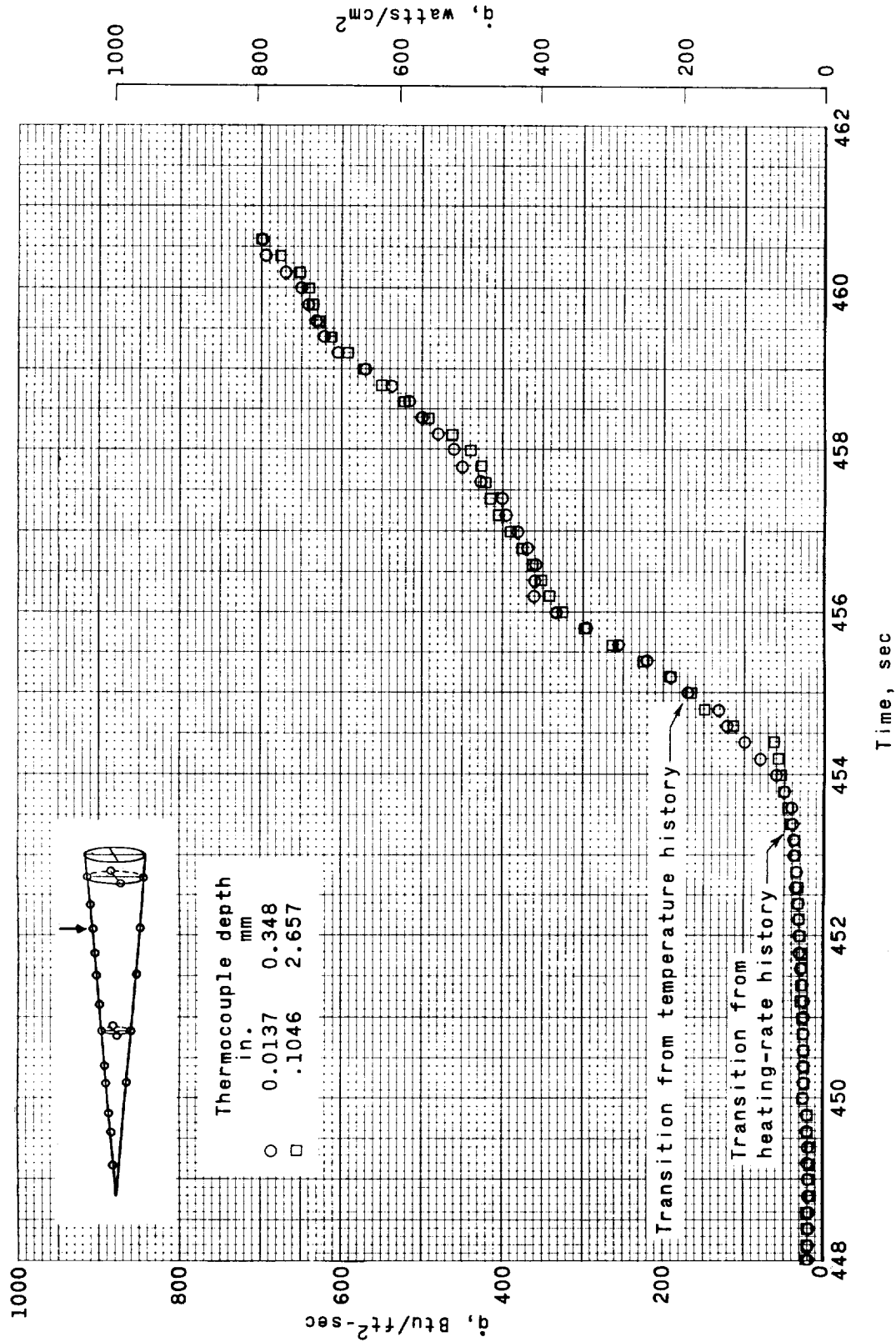
(a) Station 101.6 cm (40.0 in.).

Figure 10.- Typical heating-rate histories at four axial locations ($\phi = 0^\circ$).



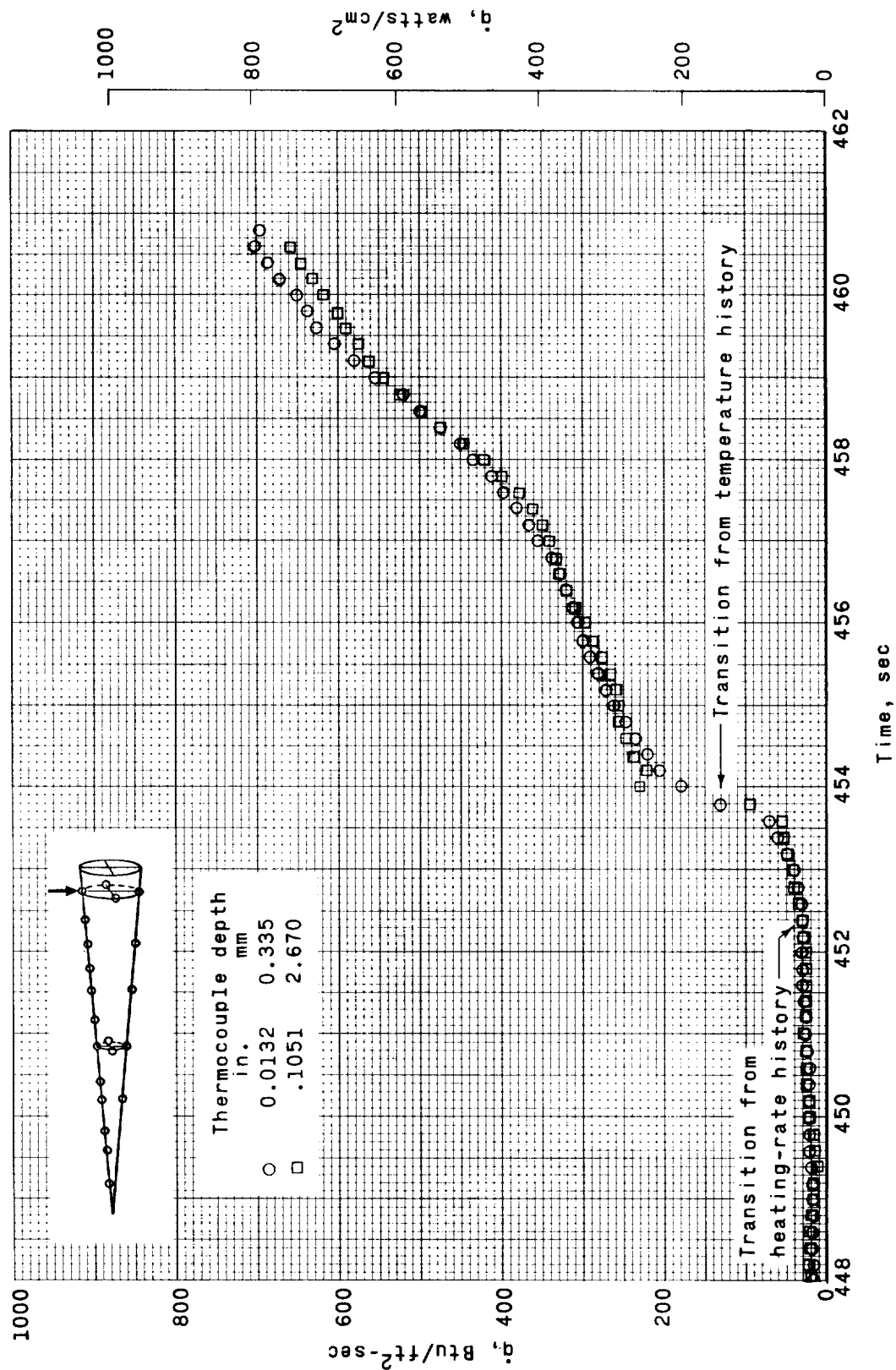
(b) Station 215.9 cm (85.0 in.).

Figure 10.- Continued.



(c) Station 307.3 cm (121.0 in.).

Figure 10.- Continued.



(d) Station 365.7 cm (144.0 in.).

Figure 10.- Concluded.

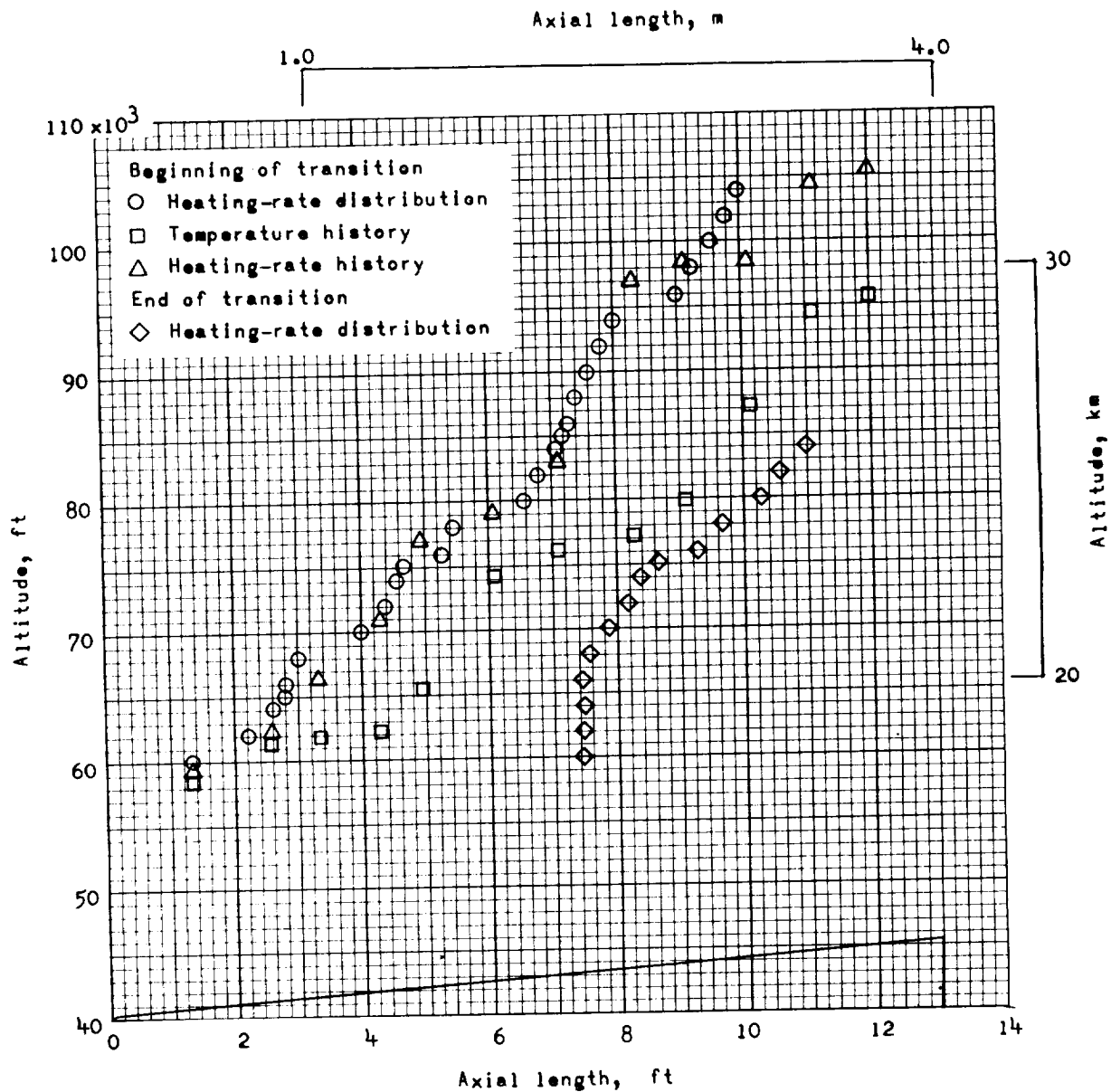


Figure 11.- Comparison of transition locations from heating-rate histories, temperature histories, and heating-rate distributions.

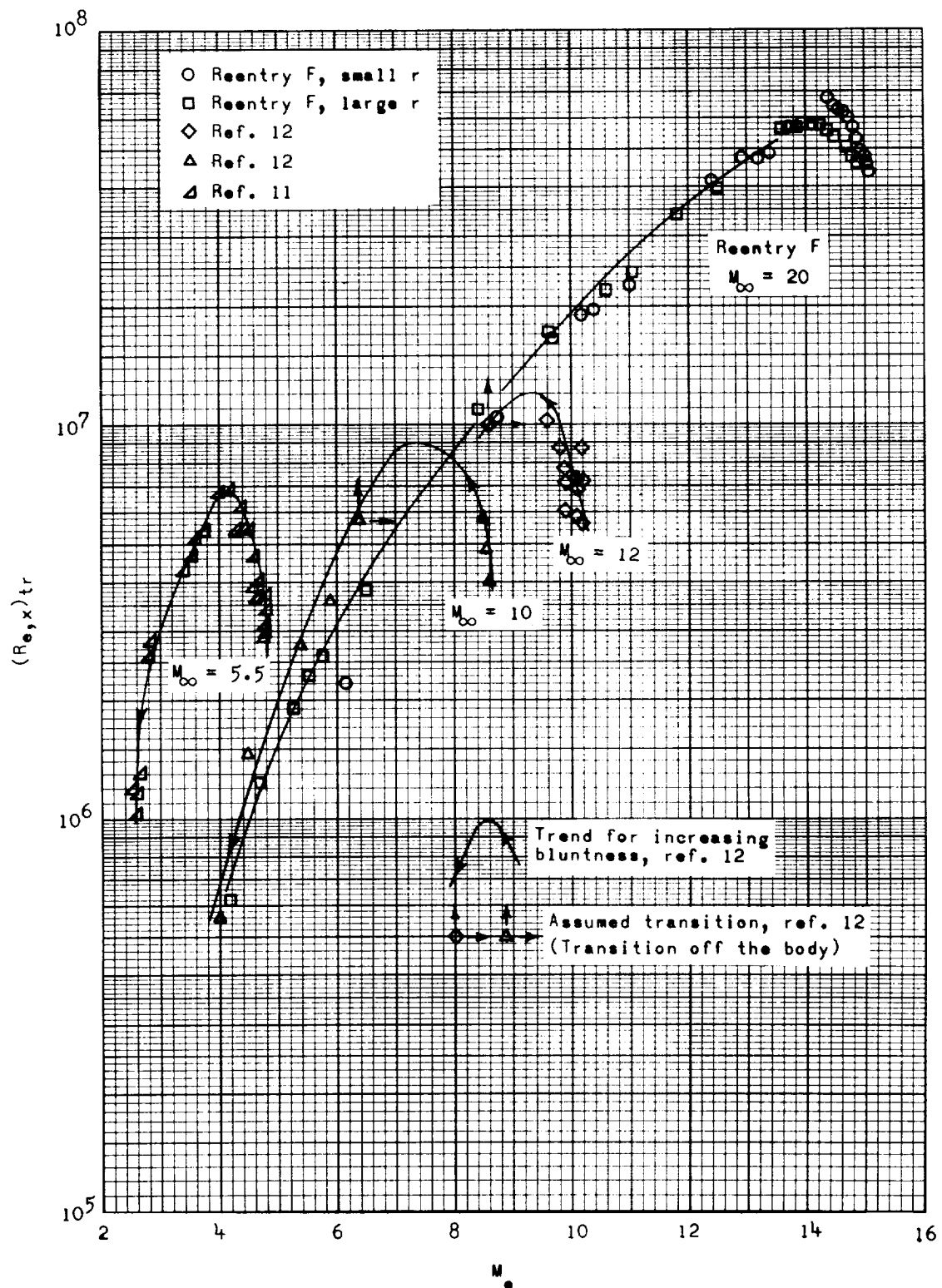


Figure 12.- Reynolds numbers at beginning of transition.

~~CONFIDENTIAL~~

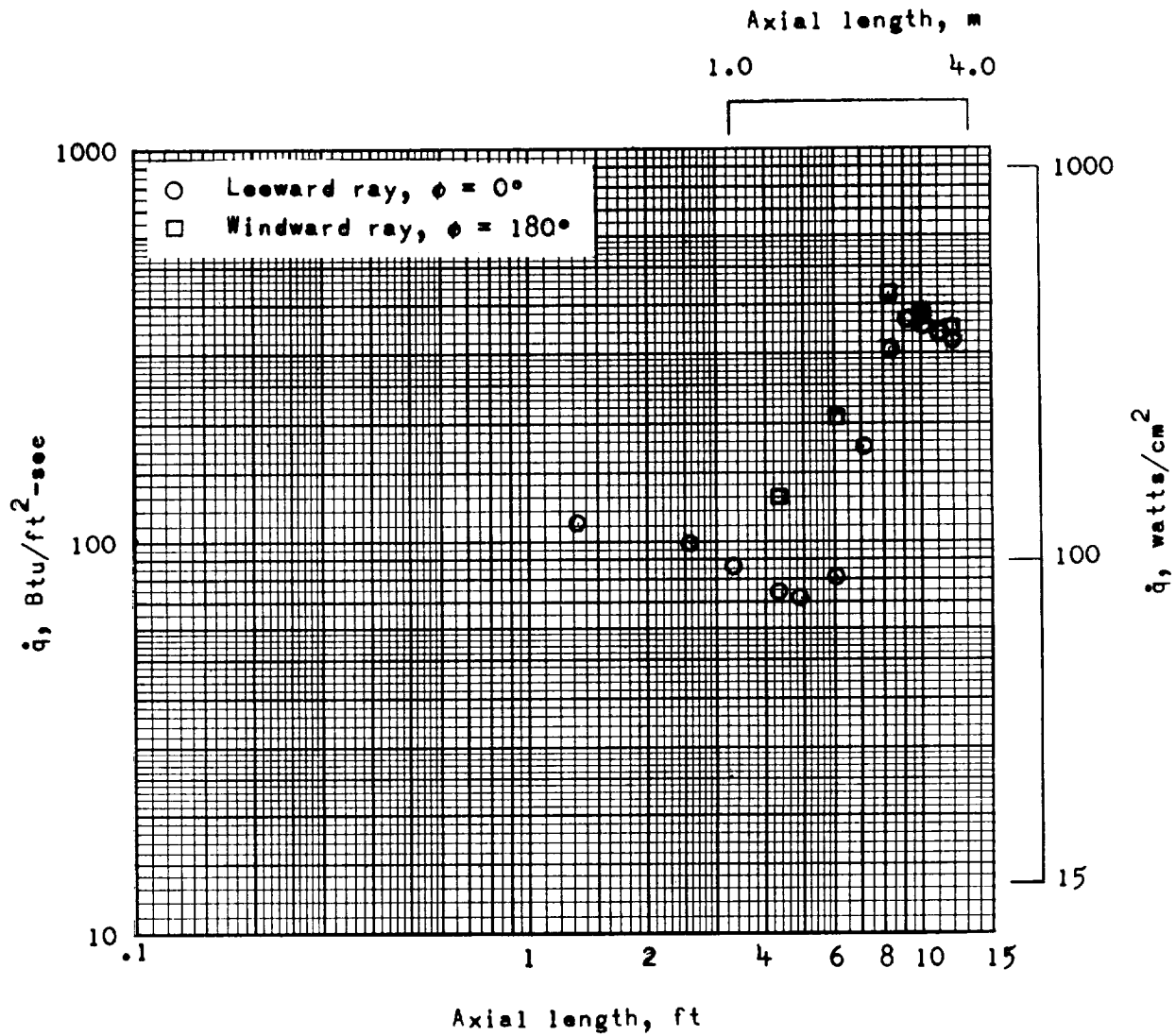


Figure 13.- Heating-rate distributions for leeward and windward rays for altitude of 23.165 km (76 000 ft).

~~CONFIDENTIAL~~

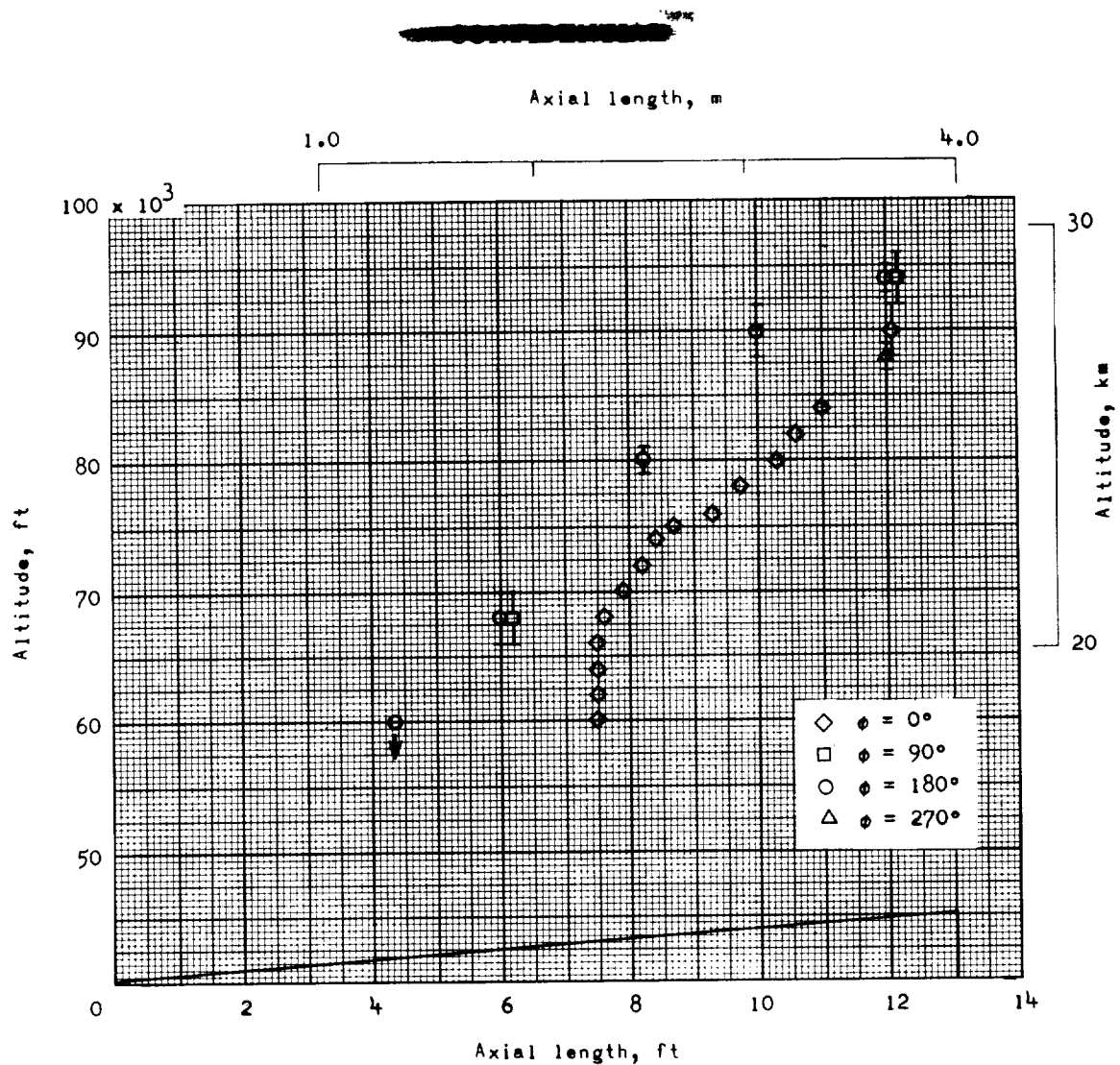


Figure 14.- Axial distribution of point of peak heating (end of transition).

- 90 000 ft (27.432 km)
- 80 000 ft (24.384 km)
- ◇ 68 000 ft (20.726 km)
- △ 60 000 ft (18.288 km)

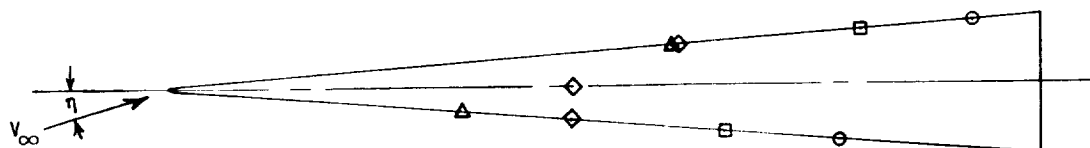


Figure 15.- Spatial distribution of end of transition.